Singlet-doublet fermion Dark Matter with Dirac neutrino mass, $(g - 2)_\mu$ and $\Delta N_{\rm eff}$

Debasish Borah ⓘ,[a] **Satyabrata Mahapatra** ⓘ,[b] **Dibyendu Nanda** ⓘ,[c]
Sujit Kumar Sahoo ⓘ[d] **and Narendra Sahu** ⓘ[d]

[a]*Department of Physics, Indian Institute of Technology Guwahati,*
 Assam 781039, India
[b]*Department of Physics and Institute of Basic Science, Sungkyunkwan University,*
 Suwon 16419, Korea
[c]*School of Physics, Korea Institute for Advanced Study,*
 Seoul 02455, Korea
[d]*Department of Physics, Indian Institute of Technology Hyderabad,*
 Kandi, Sangareddy 502285, Telangana, India

 E-mail: dborah@iitg.ac.in, satyabrata@g.skku.edu, dnanda@kias.re.kr,
 ph21resch11008@iith.ac.in, nsahu@phy.iith.ac.in

Abstract: We study the possibility of generating light Dirac neutrino mass via scotogenic mechanism where singlet-doublet fermion Dark Matter (DM) plays non-trivial role in generating one-loop neutrino mass, anomalous magnetic moment of muon: $(g - 2)_\mu$ as well as additional relativistic degrees of freedom $\Delta N_{\rm eff}$ within reach of cosmic microwave background (CMB) experiments. We show that the Dirac nature of neutrinos can bring interesting correlations within the parameter space satisfying the $(g - 2)_\mu$, DM relic density and the effective relativistic degrees of freedom $\Delta N_{\rm eff}$. While we stick to thermal singlet-doublet DM with promising detection prospects, both thermal and non-thermal origin of $\Delta N_{\rm eff}$ have been explored. In addition to detection prospects of the model at DM, $(g - 2)_\mu$ and other particle physics experiments, it remains verifiable at future CMB experiments like CMB-S4 and SPT-3G.

Contents

1 Introduction

The mysteries of the Universe have always motivated us to explore the fundamental aspects of physics beyond the standard model(SM) of particle physics. The prime among them are understanding the dark matter (DM) component, the origin of neutrino mass and the anomalous magnetic moment of muon: $(g-2)_\mu$, to count a few, that challenge the phenomenological success of the SM. DM is particularly puzzling because we can only detect its presence through its gravitational effects on visible matter and the structure of the Universe. Studies using satellites like WMAP and PLANCK [1, 2] measuring the anisotropies in the cosmic microwave background(CMB) have shown that DM makes up about 85% of all matter and approximately 27% of the Universe's total energy density. The current abundance of DM is frequently expressed in terms of the density parameter Ω_{DM} and the normalized Hubble parameter h, defined as the Hubble parameter divided by 100 km s^{-1}Mpc^{-1}, yielding $\Omega_{\mathrm{DM}}h^2 = 0.120 \pm 0.001$ at a 68% C.L.. Despite its significant role in cosmology, DM remains elusive, as no known SM particles fit the criteria of being DM. This has led researchers to consider new theories beyond the SM, with the weakly interacting massive particle (WIMP) model being one of the most studied. The WIMP model suggests that DM particles could have masses and interaction strengths similar to those of electroweak particles, potentially explaining the observed abundance of DM through a process known as thermal freeze-out. However, despite extensive searches, no direct evidence of DM has been found, placing strict limits on the possible interactions between DM and ordinary matter. A comprehensive assessment of WIMP-type DM models is available in a recent review [3, 4].

In addition to DM, SM also fails to explain the origin of neutrino mass and mixing, which has been confirmed by neutrino oscillation experiments [5–9]. Neutrino oscillation data only captures the differences in the squared masses of neutrinos($\Delta m_{\mathrm{atm}}^2 = (2.358-2.544) \times 10^{-3}$ eV^2 and $\Delta m_{\mathrm{sol.}}^2 = (6.79 - 8.01) \times 10^{-5}$ eV^2), while cosmological data place limits on their absolute mass scale ($|\sum_i m_{\nu_i}| \leq 0.12$ eV) [10]. However the question of whether neutrinos are Dirac or Majorana particles remains open. While neutrino oscillation experiments cannot settle this, searches for neutrino-less double beta decay might confirm the Majorana nature of neutrinos. But so far, no evidence has been found leaving the Majorana nature of light neutrinos unverified. This has kindled increased interest in exploring the plausibility of light Dirac neutrinos. While traditional Dirac neutrino mass models built on the seesaw mechanism have been discussed in [11–13], alternative scenarios outlining the possibility of light Dirac neutrino mass can be found in [14–21] and related references.

Another unresolved issue within the SM is the anomalous magnetic moment of the muon defined as $a_\mu = (g-2)_\mu / 2$. The quantity $\Delta a_\mu = a_\mu^{\mathrm{exp}} - a_\mu^{\mathrm{SM}}$, measures the difference between the muon's measured magnetic moment and the value predicted by the SM. Recent experiments have reported a discrepancy between the measured and predicted values of $(g-2)_\mu$, suggesting the possibility of new physics beyond the SM [22–44]. The 2021 analysis conducted by the $(g-2)_\mu$ collaboration, with the Fermilab's E989 experiment result in conjunction with the prior results from Brookhaven, revealed a discrepancy of 4.2σ. A more recent analysis by the same collaboration [45] has yielded $\Delta a_\mu = 249(48) \times 10^{-11}$, indicating a discrepancy of 5.1σ from the SM predicted value. However, it is important to note that, due to the non-perturbative nature of the low-energy strong interaction, the uncertainty in a_μ^{SM} is primarily dominated by contributions from hadronic vacuum polarization (HVP), which is difficult to calculate precisely. Despite recent measurements [46, 47] that have reduced this uncertainty, there is still no conclusive evidence, leaving room for alternative BSM explanations. A review of such new physics explanations for $(g-2)_\mu$ can be found in [48–50].

Although the origin of the aforementioned puzzles remain unknown, in this paper we aim to propose a concise model that explains them within a common framework. We explore a WIMP-like fermionic DM scenario, involving a vector-like singlet and a doublet [51, 52]. The rationale for exploring this particular fermionic configuration is well-established as in singlet-doublet setups, there is mixing between the neutral component of the doublet and the singlet through the Yukawa interaction and DM manifests as a mixed state [51–80], satisfying appropriate relic density across a broad range of masses while adhering to direct search limits, which is not the case for purely a singlet or a doublet scenario. Additionally, we extend this model with one scalar and three right-handed neutrinos (ν_{R_i}) to incorporate the Dirac mass of light neutrinos in a scotogenic setup, offering complementary cosmological probes in CMB measurements in contrast to the singlet-doublet fermionic DM setups considered in literature in connection to Majorana neutrino masses [75–81]. The presence of right handed neutrinos in our model potentially introduce extra light degrees of freedom. Current CMB experiments have placed stringent constraints on effective light degrees of freedom during the recombination era ($z \sim 1100$), yielding $\mathrm{N}_{\mathrm{eff}} = 2.99^{+0.34}_{-0.33}$ at 2σ aligning with SM predictions of $\mathrm{N}_{\mathrm{eff}}^{\mathrm{SM}} = 3.046$ [1, 2]. Future experiments like CMB-S4 aim for unprecedented sensitivity, targeting $\Delta \mathrm{N}_{\mathrm{eff}} = 0.06$ at 2σ CL [82]. This precision measurement can scrutinize

Gauge	Fermion Fields					Scalar	
Group	L_L	l_R	Ψ	χ	ν_R	H	ϕ
$SU(2)_L$	2	1	2	1	1	2	1
$U(1)_Y$	-1	-2	-1	0	0	1	0
Z_4	$-i$	$-i$	-1	-1	i	$+1$	i

Table 1. Particles and their charge assignments in our setup.

scenarios featuring light degrees of freedom that we have. Due to the minimality of the framework, which offers a unified resolution to the aforementioned challenges, it reveals a strong correlation among the model parameters, making the model extremely predictive at various present and future experiments.

The rest of the paper is organized as follows. In section 2, we discuss a most minimal extended version of the singlet-doublet fermionic model to incorporate radiative Dirac neutrino mass. In section 3, we show the generation of Dirac neutrino mass at one-loop level. In section 4, we analyse the bounds from $(g-2)_\mu$ on our model parameters followed by the lepton flavour violation constraint. In section 5, we discuss the relic density of DM and direct detection constraints. In section 6, we discuss the details of ΔN_{eff} and finally conclude in section 7.

2 The model

As discussed in the introduction, to generate the Dirac mass of light neutrinos in a scotogenic setup we augment the SM fermion content by adding 2 generations of vector-like fermion doublet $\Psi = (\psi^0 \ \psi^-)^T$ (with hypercharge $Y = -1$, where we use the electromagnetic charge definition $Q = T_3 + Y/2$) and 2 generations of vector-like singlet fermion χ with hypercharge $Y = 0$, together with three copies of right handed neutrinos ν_R. In addition to the singlet-doublet fermionic extension of SM, we introduce another singlet complex scalar $\phi(= \frac{\phi_1 + i\phi_2}{\sqrt{2}})$. With this particle content, we introduce a discrete Z_4 symmetry, where this new symmetry is responsible for forbidding the tree level realization of Dirac neutrino mass and the Majorana mass of ν_R. The charge assignments of the particles under the imposed symmetries are shown in table. 1.

The relevant Lagrangian of the model guided by the imposed symmetry is given by:

$$\mathcal{L} \supset i\overline{\Psi}\gamma^\mu D_\mu \Psi + i\overline{\chi}\gamma^\mu \partial_\mu \chi - M_\Psi \overline{\Psi}\Psi - M_\chi \overline{\chi}\chi$$
$$-y\overline{\Psi}\tilde{H}\chi - \lambda_\psi \overline{L}\phi\Psi - \lambda_\chi \overline{\nu_R}\phi^\dagger \chi + h.c., \tag{2.1}$$

where $D_\mu = \partial_\mu - g_1 \frac{\tau_i}{2} W_\mu^i - g_2 \frac{Y}{2} B_\mu$. For simplicity, we suppress the generation indices in the Lagrangian. The scalar potential involving H and ϕ which satisfy Z_4 symmetry is given by:

$$V_{H,\phi} = -\mu_H^2 (H^\dagger H) + \lambda_H (H^\dagger H)^2$$
$$+M_\phi^2 (\phi^\dagger \phi) + \lambda_\phi (\phi^\dagger \phi)^2 + \lambda_{\phi H}(\phi^\dagger \phi)(H^\dagger H) \tag{2.2}$$

In our setup, we choose $M_\phi^2 > 0$ such that ϕ doesn't acquire any vacuum expectation value (VEV), thus forbidding any mixing between ν_R and χ. Moreover, the SM Higgs H

is inert under Z_4 symmetry and hence can not lead to spontaneous Z_4 breaking together with electroweak symmetry breaking.

In order to generate the Dirac mass of neutrinos, one has to break Z_4 symmetry. In order to do so, we add a soft term $\frac{1}{2}\mu_\phi^2 \left(\phi^2 + (\phi^\dagger)^2 \right)$ in the scalar potential which breaks Z_4 symmetry explicitly. After electroweak symmetry breaking, SM Higgs acquires a VEV. In presence of the soft term, the masses of ϕ_1 and ϕ_2 can be written as,

$$
\begin{aligned}
M_{\phi_1}^2 &= M_\phi^2 + \mu_\phi^2 + \frac{1}{2}\lambda_{\phi H}v^2 \\
M_{\phi_2}^2 &= M_\phi^2 - \mu_\phi^2 + \frac{1}{2}\lambda_{\phi H}v^2
\end{aligned}
\tag{2.3}
$$

and the mass squared difference, $\Delta M_\phi^2 = M_{\phi_1}^2 - M_{\phi_2}^2 = 2\mu_\phi^2$. We will show that ΔM_ϕ^2 is responsible for generating Dirac mass of neutrino at one-loop level in section 3. The Higgs VEV also leads to mixing between the neutral component of doublet ψ^0 and χ, giving rise to two singlet-doublet admixed mass eigenstates. The mass terms for these fields can then be written together as follows:

$$
\begin{aligned}
-\mathcal{L}_{\text{mass}}^{VF} &= M_\Psi \overline{\psi^0}\psi^0 + M_\Psi \psi^+\psi^- + M_\chi \overline{\chi}\chi + \frac{yv}{\sqrt{2}}\,\overline{\psi^0}\,\chi + \frac{yv}{\sqrt{2}}\,\overline{\chi}\,\psi^0 \\
&= \overline{\left(\psi^0 \; \chi \right)}\begin{pmatrix} M_\psi & yv/\sqrt{2} \\ yv/\sqrt{2} & M_\chi \end{pmatrix}\begin{pmatrix} \psi^0 \\ \chi \end{pmatrix} + M_\Psi \psi^+\psi^-.
\end{aligned}
\tag{2.4}
$$

Denoting the mass eigenstates as χ_1 and χ_2 and θ to be the mixing angle, the flavour basis, $\left(\psi^0 \; \chi \right)^T$ is related to the physical basis, $\left(\chi_1 \; \chi_2 \right)^T$ through the orthogonal transformation:

$$
\begin{pmatrix} \psi^0 \\ \chi \end{pmatrix} = \mathcal{O}\begin{pmatrix} \chi_1 \\ \chi_2 \end{pmatrix} = \begin{pmatrix} \cos\theta & -\sin\theta \\ \sin\theta & \cos\theta \end{pmatrix}\begin{pmatrix} \chi_1 \\ \chi_2 \end{pmatrix},
\tag{2.5}
$$

where the mixing angle is given by:

$$
\tan 2\theta = \frac{\sqrt{2}yv}{M_\Psi - M_\chi}.
\tag{2.6}
$$

From eq. (2.4), we get the mass eigenvalues of the physical states to be:

$$
\begin{aligned}
M_{\chi_1} &= M_\Psi \cos^2\theta + \frac{yv}{\sqrt{2}}\sin 2\theta + M_\chi \sin^2\theta, \\
M_{\chi_2} &= M_\Psi \sin^2\theta - \frac{yv}{\sqrt{2}}\sin 2\theta + M_\chi \cos^2\theta
\end{aligned}
\tag{2.7}
$$

with a mass-splitting $\Delta M = M_{\chi_1} - M_{\chi_2}$.

One important thing to note is that the eqs. (2.1) and (2.2) possess an unbroken Z_2 symmetry under which Ψ, χ, ϕ are odd while all other particles are even. This remnant symmetry survives even after Z_4 is softly broken by the quadratic terms mentioned above. While our choice of soft-breaking terms has resulted in this remnant symmetry, one can also impose it as an additional symmetry while keeping the phenomenology unaltered. We assume a mass hierarchy: $M_{\chi_1} > M_{\phi_1} > M_{\phi_2} > M_{\chi_2}$. As a result, the lightest Z_2 odd particle χ_2, which is dominantly a singlet fermion χ with a small admixture of the doublet
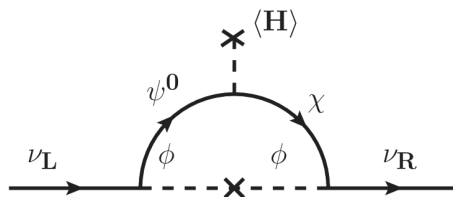
Figure 1. Dirac Neutrino Mass generation at one-loop level.

fermion Ψ, behaves as a DM. In eq. (2.1), the term $\bar{L}\phi\Psi$ is responsible for $(g-2)_\mu$, the details of which are discussed in section 4.

In order to satisfy the neutrino oscillation data, a minimum of two generations of singlet-doublet fermions are required. The consideration of multiple generations of singlet-doublet fermions is also motivated in the context of addressing the CDF-II W-mass anomaly, as explored recently in [80]. However, in our present work, the role of heavier generation of singlet-doublet fermions is only to generate the correct neutrino data. For rest of the phenomenology discussed here, we focus only on the lighter generation of singlet-doublet fermions. This choice is justified by considering a mass difference of the order of $\mathcal{O}(10^3)\,\text{GeV}$ between the two generations. Consequently, the presence of the heavier generation has negligible impact on the DM phenomenology and the ΔN_{eff} analysis, as we disregard inter-generational mixing among these dark fermions. Furthermore, assuming maximal mixing between the singlet and doublet fermions of the heavier generation allows us to fine-tune the corresponding couplings to leptons to smaller values, while being consistent with the neutrino data. This ensures that any additional contribution from the heavier generation of singlet-doublet fermions to $(g-2)_\mu$ and lepton flavor violation (LFV) processes remain suppressed when compared to the contributions from the lighter generation.

Thus the relevant parameters of the model are the masses $\{M_{\chi_2}, \Delta M(= M_{\chi_1} - M_{\chi_2}), M_{\psi^-},$ $M_{\phi_1}, \Delta M_1(= M_{\phi_2} - M_{\chi_2})\}$, the mixing angle $(\sin\theta)$, and the couplings $\{\lambda_\psi, \lambda_\chi\}$. These parameters collectively influence various aspects including the neutrino mass generation, the contribution to muon magnetic moment, DM annihilation and co-annihilation dynamics as well as the thermalisation of ν_R acting as dark radiation and providing additional complementary cosmological probe for this scenario in terms of ΔN_{eff}, which we discuss in details in the subsequent sections of this article.

3 Dirac neutrino mass

As discussed in the previous section, the Z_4 symmetry is explicitly broken by the term $\frac{1}{2}\mu_\phi^2\left(\phi^2 + (\phi^\dagger)^2\right)$. This leads to the realisation of Dirac neutrino mass operator $\bar{L}\tilde{H}\nu_R$ at one-loop level with the singlet-doublet fermions(ψ^0, χ) and the singlet scalar ϕ running in the loop as shown in figure 1.

The one-loop light neutrino mass can be estimated to be:

$$(M_\nu)_{\alpha\beta} = \frac{\mu_\phi^2}{16\pi^2} \sum_i \left((\lambda_\psi)_{i\alpha}\right)^T \left(\Delta M \sin(2\theta)\, F(M_{\chi_1}, M_{\chi_2}, M_{\phi_1}, M_{\phi_2})\right)_i I_{ii}(\lambda_\chi)_{i\beta} \qquad (3.1)$$

	Set 1			**Set 2**	
Parameters	1st Generation	2nd Generation	Parameters	1st Generation	2nd Generation
$\sin\theta$	5.8×10^{-8}	0.7	$\sin\theta$	0.0053	0.7
M_{χ_1} (GeV)	519	3638	M_{χ_1} (GeV)	867	3207
M_{χ_2} (GeV)	180	2638	M_{χ_2} (GeV)	859	2207
λ_{ψ_e}	1.38×10^{-7}	1.64×10^{-7}	λ_{ψ_e}	8.30×10^{-7}	5.97×10^{-5}
λ_{ψ_μ}	0.0358	0.0031	λ_{ψ_μ}	0.0485	1.64×10^{-5}
λ_{ψ_τ}	0.0075	0.0090	λ_{ψ_τ}	0.0295	0.04
λ_{χ_e}	0.0264	4.96×10^{-9}	λ_{χ_e}	0.0006	4.87×10^{-8}
λ_{χ_μ}	0.0051	7.40×10^{-8}	λ_{χ_μ}	4.98×10^{-4}	1.00×10^{-9}
λ_{χ_τ}	2.84	5.05×10^{-9}	λ_{χ_τ}	5.71×10^{-5}	4.38×10^{-8}

Table 2. Two sets of benchmark points for 1st and 2nd Generation singlet-doublet fermions are given. Where for the Set 1, $M_{\phi_2} = 532.14$ GeV and two non zero neutrino mass eigen values are $\sqrt{\Delta m_{\text{atm}}^2} = 4.94 \times 10^{-11}$ GeV and $\sqrt{\Delta m_{\text{sol}}^2} = 8.63 \times 10^{-12}$ GeV. Similarly, for the Set 2, $M_{\phi_2} = 711$ GeV, $\sqrt{\Delta m_{\text{atm}}^2} = 4.95 \times 10^{-11}$ GeV and $\sqrt{\Delta m_{\text{sol}}^2} = 8.58 \times 10^{-12}$ GeV.

where i represents the generation index of singlet-doublet fermion, α and β represent lepton flavour indices, I is the 2×2 identity matrix and $F(M_{\chi_1}, M_{\chi_2}, M_{\phi_1}, M_{\phi_2})$ is the loop factor and is given by,

$$F(M_{\chi_1}, M_{\chi_2}, M_{\phi_1}, M_{\phi_2}) = \frac{(M_{\chi_1} - 4M_{\chi_2}) M_{\chi_2}^3 \log\left(\frac{M_{\chi_2}^2}{M_{\chi_1}^2}\right)}{\left(M_{\chi_1}^2 - M_{\chi_2}^2\right)\left(M_{\phi_1}^2 - M_{\chi_2}^2\right)\left(M_{\phi_2}^2 - M_{\chi_2}^2\right)} \tag{3.2}$$
$$+ \frac{1}{M_{\phi_1}^2 - M_{\phi_2}^2}\left[\frac{M_{\phi_1}^2 \left(M_{\chi_1} M_{\chi_2} - 4M_{\phi_1}^2\right) \log\left(\frac{M_{\phi_1}^2}{M_{\chi_1}^2}\right)}{\left(M_{\chi_1}^2 - M_{\phi_1}^2\right)\left(M_{\phi_1}^2 - M_{\chi_2}^2\right)} - \frac{M_{\phi_2}^2 \left(M_{\chi_1} M_{\chi_2} - 4M_{\phi_2}^2\right) \log\left(\frac{M_{\phi_2}^2}{M_{\chi_1}^2}\right)}{\left(M_{\chi_1}^2 - M_{\phi_2}^2\right)\left(M_{\phi_2}^2 - M_{\chi_2}^2\right)}\right]$$

For two generations of singlet-doublet fermion, the eq. (3.1) can be written in a matrix form as,

$$(M_\nu)_{3\times3} = \begin{pmatrix} M_{ee} & M_{e\mu} & M_{e\tau} \\ M_{\mu e} & M_{\mu\mu} & M_{\mu\tau} \\ M_{\tau e} & M_{\tau\mu} & M_{\tau\tau} \end{pmatrix} = \sum_{i=1}^{2} f^i \begin{pmatrix} \lambda_{\psi_{ie}}\lambda_{\chi_{ie}} & \lambda_{\psi_{ie}}\lambda_{\chi_{i\mu}} & \lambda_{\psi_{ie}}\lambda_{\chi_{i\tau}} \\ \lambda_{\psi_{i\mu}}\lambda_{\chi_{ie}} & \lambda_{\psi_{i\mu}}\lambda_{\chi_{i\mu}} & \lambda_{\psi_{i\mu}}\lambda_{\chi_{i\tau}} \\ \lambda_{\psi_{i\tau}}\lambda_{\chi_{ie}} & \lambda_{\psi_{i\tau}}\lambda_{\chi_{i\mu}} & \lambda_{\psi_{i\tau}}\lambda_{\chi_{i\tau}} \end{pmatrix}$$
$$= \sum_{i=1}^{2} \begin{pmatrix} \lambda_{\psi_{ie}} \\ \lambda_{\psi_{i\mu}} \\ \lambda_{\psi_{i\tau}} \end{pmatrix} f^i \begin{pmatrix} \lambda_{\chi_{ie}} & \lambda_{\chi_{i\mu}} & \lambda_{\chi_{i\tau}} \end{pmatrix} \tag{3.3}$$

where $f^i = \frac{\mu_\phi^2}{16\pi^2}\left(\Delta M^i \sin 2\theta^i \ F(M_{\chi_1}^i, M_{\chi_2}^i, M_{\phi_1}, M_{\phi_2})\right)$.

Imposing the bound from cosmological data on the sum of light neutrino masses, $\sum m_i < 0.12$ eV and the neutrino oscillation data ($\Delta m_{\text{atm}}^2 = (2.358 - 2.544) \times 10^{-3}$ eV^2 and $\Delta m_{\text{sol.}}^2 = (6.79 - 8.01) \times 10^{-5}$ eV^2) at 3σ C.L., we put stringent constraints on the parameters governing the generation of the light Dirac neutrino mass. Two benchmark values are given in table 2.

Model Parameters	Range for the scan	
	1st Generation	2nd Generation
$\sin\theta$	$[10^{-8}, 0.3]$	0.7
$\Delta M = M_{\chi_1} - M_{\chi_2}$ (GeV)	$[1, 10^3]$	$[500, 10^3]$
$\Delta M_1 = M_{\phi_2} - M_{\chi_2}$ (GeV)	$[1, 600]$	−
M_{χ_2} (GeV)	$[1, 10^3]$	$[2000, 10^4]$
λ_{ψ_e}	$[10^{-8}, 10^{-5}]$	$[10^{-1}, 10^{-7}]$
λ_{ψ_μ}	$[1, 10^{-3}]$	$[10^{-1}, 10^{-7}]$
λ_{ψ_τ}	$[10^{-1}, 10^{-4}]$	$[10^{-1}, 10^{-7}]$
λ_{χ_e}	$[10^{-7}, \sqrt{4\pi}]$	$[10^{-10}, 10^{-7}]$
λ_{χ_μ}	$[10^{-7}, \sqrt{4\pi}]$	$[10^{-10}, 10^{-7}]$
λ_{χ_τ}	$[10^{-7}, \sqrt{4\pi}]$	$[10^{-10}, 10^{-7}]$

Table 3. Range of model parameters used for the numerical scan. We fix the mass difference, $M_{\phi_1} - M_{\phi_2} = 1$ GeV.
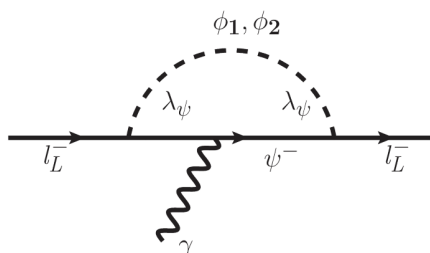
Figure 2. Feynman diagram giving rise to $(g-2)_\mu$ and lepton flavour violation.

For simplicity, we fixed $(M_{\phi_1} - M_{\phi_2})$ to be $1\,\text{GeV}$ and the coupling parameters of the second generation singlet-doublet fermions comparably small to that of first generation. It is noteworthy that this constraint not only establishes a distinctive correlation between the neutrino mass and the $(g-2)_\mu$, but also forges intriguing links between the DM phenomenology and the model's predictions regarding ΔN_{eff}.

4 Anomalous magnetic moment of muon: $(g-2)_\mu$

The anomalous magnetic moment of the muon, often denoted as $(g-2)_\mu$, refers to the difference between the muon's actual magnetic moment and the value predicted by the Dirac equation within the framework of quantum electrodynamics (QED). This deviation arises due to quantum fluctuations and interactions with virtual particles in the vacuum.

In our setup, the new positive contribution to the $(g-2)_\mu$ comes from the one loop diagram with the charged doublet fermion ψ^- and the singlet scalars $\phi_{1,2}$ in the loop. This
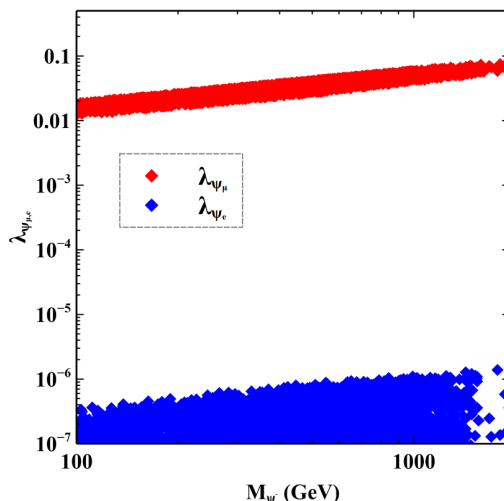
Figure 3. The allowed region for $(g-2)_\mu$ is depicted by the red coloured points in the parameter space of λ_{ψ_μ} and M_{ψ^-}. The values of λ_{ψ_e} consistent with the LFV constraints are also projected in the same plane by the blue points. The details of the LFV decay are discussed in the next section.

contribution to $(g-2)_\mu$ is given by [49],

$$\Delta a_\mu = \frac{m_\mu^2 \left(y_\psi\right)_\mu^2}{8\pi^2} \int_0^1 dx \left[I_1^+(x, M_{\psi^-}, M_{\phi_1}) - I_1^-(x, M_{\psi^-}, M_{\phi_2}) \right] \tag{4.1}$$

Where

$$I_1^{(\pm)}(x, m_1, m_2) = \frac{x^2 \left(1 - x \pm \frac{m_1}{m_\mu}\right)}{\left((1-x)\left(m_2^2 - x m_\mu^2\right) + x m_1^2\right)} \tag{4.2}$$

In figure 3, we showcase the parameter space satisfying correct Δa_μ by the red coloured points, in the plane of λ_{Ψ_μ} and M_{ψ^-} with M_{ϕ_1} varying in a range as mentioned in table 3. We first carried out a numerical scan varying the model parameters in the range as shown in table 3 and found the parameter space that satisfies the correct neutrino mass criteria. The same parameter set is then used for the scan to check the constraint from $(g-2)_\mu$.

Clearly, we can see that λ_{Ψ_μ} is constrained in the interval $[0.01, 0.1]$ while imposing the lower bound on the charged fermion doublet mass to be $M_{\Psi^-} > 102.7\,\mathrm{GeV}$ from LEP [83]. As the mass of the particles in the loop suppresses the contribution to $(g-2)_\mu$, the corresponding coupling λ_{ψ_μ} has to increase. This can be easily seen from figure 3.

4.1 Lepton flavour violation

The decay involving charged lepton flavour violation (LFV) is a significant process for investigating physics beyond the SM. Within the SM framework, this process takes place at the one-loop level and is greatly suppressed due to the minuteness of neutrino masses and therefore remains far beyond the current experimental sensitivities [84]. Consequently, any future detection of LFV decays, such as $\mu \to e\gamma$, would unquestionably constitute evidence of physics beyond SM. In our current model, this additional new physics contribution

comes from the same diagram as shown in figure 2 with leptons of two different flavours in the external legs. The branching ratio for $\mu \to e\gamma$ is given by [49]:

$$\text{BR}(\mu^- \to e^-\gamma) = \frac{3\alpha}{16\pi G_F^2} \left| \lambda_{\psi_\mu} \lambda_{\psi_e} I(M_{\psi^-}, M_\phi) \right|^2, \tag{4.3}$$

where

$$I(M_{\psi^-}, M_\phi) = \int_0^1 dx \int_0^{1-x} dy \left[I_2^+(x, y, M_{\psi^-}, M_{\phi_1}) - I_2^-(x, y, M_{\psi^-}, M_{\phi_2}) \right]$$

and

$$I_2^{(\pm)}(x, y, m_1, m_2) = \frac{x \left(y + (1 - x - y)\frac{m_e}{m_\mu} \right) \pm (1 - x)\frac{m_1}{m_\mu}}{-xym_\mu^2 - x(1 - x - y)m_e^2 + xm_2^2 + (1 - x)m_1^2}.$$

Given the existing constraints on λ_{ψ_μ} and M_{ψ^-,ϕ_1} from the $(g - 2)_\mu$ experiment, and taking into account the upper limit on $Br(\mu \to e\gamma)$ set by MEG [84], we can establish an upper bound for λ_{ψ_e}. This is shown in figure 3 by the blue coloured points. As we can see, it puts a conservative upper limit that λ_{ψ_e} must be less than 10^{-6} for $M_{\psi^-} \in [100, 1800]$ GeV in order to remain consistent with the MEG constraint.

5 Dark Matter phenomenology

As outlined in section 2, χ_2, being the lightest odd particle under Z_2 symmetry, attains stability and emerges as a plausible DM candidate in our framework. Being an admixed state of a singlet and a doublet fermion, its thermalization and relic abundance are crucially governed by the Yukawa and gauge interactions. Thus its relic density is determined by the process of thermal freeze-out, wherein the primary mechanisms involve the annihilation of DM into SM particles and ν_R, along with co-annihilation among the dark sector constituents χ_2, χ_1, ϕ_1, ϕ_2, and ψ^-.

Before delving into the phenomenology of DM, it is important to note that the inclusion of ν_R and $\phi_{1,2}$ in this setup, and their significant involvement in the genesis of neutrino mass at one-loop, not only offers an additional cosmological probe to validate the model but also alters the conventional outcomes typically observed in the study of Dirac fermionic singlet-doublet DM alone as explored in [52, 76]. As in section 6, we will thoroughly examine the ΔN_{eff} component of this scenario, it is pivotal to consider whether ν_R undergoes thermalization or not because the same coupling plays a crucial role in determining DM relic density.

The production of RHNs (ν_{R_i}) primarily depends on the coupling parameter λ_χ. This same coupling also dictates whether RHNs undergo thermalization. For values of λ_χ greater than 10^{-3}, we observe that RHNs were in thermal equilibrium with the SM bath alongside other constituents of the dark sector. Consequently, both $\phi_{1,2}$ and $\chi_{1,2}$ annihilation contribute to the production of RHNs and hence the enhancement of additional relativistic energy density. Conversely, for smaller values of λ_χ, RHNs were not in equilibrium with the SM bath, making it challenging to produce them through thermal processes. In such instances, RHNs can still be generated through non-thermal freeze-in processes, particularly via the decay of $\phi_{1,2}$ in the process $\phi_{1,2} \to \chi_2 \nu_R$.

Consequently, we categorize our analysis into two distinct cases:

(i) **Case-1**: $10^{-3} < \lambda_\chi < \sqrt{4\pi}$.

(ii) **Case-2**: $10^{-7} < \lambda_\chi \leq 10^{-3}$.

where we use $\lambda_\chi = (\lambda_{\chi e} + \lambda_{\chi \mu} + \lambda_{\chi \tau})/3$.

5.1 Relic abundance of DM

The relic density of DM in this scenario is achieved by solving the Boltzmann equation

$$\frac{dn}{dt} + 3Hn = -\langle \sigma v \rangle_{\text{eff}}(n^2 - (n^{\text{eq}})^2) \tag{5.1}$$

where $n = \sum_i n_i$ represents the total number density of all the dark sector particles and n^{eq} is the equilibrium number density. $\langle \sigma v \rangle_{\text{eff}}$ represents the effective annihilation cross-section which takes into account all number changing processes for DM freeze-out is given by:

$$
\begin{aligned}
\langle \sigma v \rangle_{\text{eff}} &= \frac{g_2^2}{g_{\text{eff}}^2}\langle \sigma v \rangle_{\chi_2 \chi_2} + \frac{g_2 g_{1,2}}{g_{\text{eff}}^2}\langle \sigma v \rangle_{\chi_2 \phi_{1,2}}(1+\Delta_{\phi_{1,2}})^{3/2}\exp(-x\Delta_{\phi_{1,2}}) \\
&\quad + \frac{g_2 g_1}{g_{\text{eff}}^2}\langle \sigma v \rangle_{\chi_2 \chi_1}(1+\Delta_{\chi_1})^{3/2}\exp(-x\Delta_{\chi_1}) \\
&\quad + \frac{g_2 g_3}{g_{\text{eff}}^2}\langle \sigma v \rangle_{\chi_2 \psi^-}(1+\Delta_{\psi^-})^{3/2}\exp(-x\Delta_{\psi^-}) + \frac{g_{\phi_{1,2}}^2}{g_{\text{eff}}^2}\langle \sigma v \rangle_{\phi_{1,2}\phi_{1,2}}(1+\Delta_{\phi_{1,2}})^3\exp(-2x\Delta_{\phi_{1,2}}) \\
&\quad + \frac{g_{\phi_{1,2}} g_1}{g_{\text{eff}}^2}\langle \sigma v \rangle_{\phi_{1,2}\chi_1}(1+\Delta_{\phi_{1,2}})^{3/2}(1+\Delta_{\chi_1})^{3/2}\exp\left(-x(\Delta_{\phi_{1,2}}+\Delta_{\chi_1})\right) \\
&\quad + \frac{g_{\phi_{1,2}} g_3}{g_{\text{eff}}^2}\langle \sigma v \rangle_{\phi_{1,2}\psi^-}(1+\Delta_{\phi_{1,2}})^{3/2}(1+\Delta_{\psi^-})^{3/2}\exp\left(-x(\Delta_{\phi_{1,2}}+\Delta_{\psi^-})\right) \\
&\quad + \frac{g_1^2}{g_{\text{eff}}^2}\langle \sigma v \rangle_{\chi_1 \chi_1}(1+\Delta_{\chi_1})^3\exp(-2x\Delta_{\chi_1}) + \frac{g_3^2}{g_{\text{eff}}^2}\langle \sigma v \rangle_{\psi^+\psi^-}(1+\Delta_{\psi^-})^3\exp(-2x\Delta_{\psi^-}) \\
&\quad + \frac{g_1 g_3}{g_{\text{eff}}^2}\langle \sigma v \rangle_{\chi_1 \psi^-}(1+\Delta_{\chi_1})^{3/2}(1+\Delta_{\psi^-})^{3/2}\exp(-x(\Delta_{\chi_1}+\Delta_{\psi^-}))
\end{aligned}
\tag{5.2}
$$

where $g_1, g_2, g_3, g_{\phi_1}$ and g_{ϕ_2} represent the internal degrees of $\chi_1, \chi_2, \psi^-, \phi_1$ and ϕ_2 respectively and Δ_i stands for the ratio $(M_i - M_{\chi_2})/M_{\chi_2}$ with M_i denoting the mass of χ_1, ψ^-, ϕ_1 and ϕ_2. Here g_{eff} is the effective degree of freedom which is given by:

$$
\begin{aligned}
g_{\text{eff}} &= g_2 + g_{\phi_{1,2}}(1+\Delta_{\phi_{1,2}})^{3/2}\exp(-x\Delta_{\phi_{1,2}}) + g_1(1+\Delta_{\chi_1})^{3/2}\exp(-x\Delta_{\chi_1}) \\
&\quad + g_3(1+\Delta_{\psi^-})^{3/2}\exp(-x\Delta_{\psi^-})
\end{aligned}
\tag{5.3}
$$

and x is the dimensionless parameter M_{χ_2}/T.

The relic density of DM χ_2 can then be evaluated as:

$$\Omega_{\chi_2}h^2 = \frac{1.09 \times 10^9 \text{GeV}^{-1}}{\sqrt{g_*}M_{Pl}}\left[\int_{x_f}^\infty dx \, \frac{\langle \sigma v \rangle_{\text{eff}}}{x^2}\right]^{-1} \tag{5.4}$$

Here $x_f = M_{\chi_2}/T_f$, and T_f denotes the freeze-out temperature of χ_2.

To gain insight into the relic density of DM and the specific influence of model parameters in achieving the observed relic density, we conducted various analyses and explored the allowed parameter space. As studied in [52, 72], the pivotal parameters governing the relic abundance
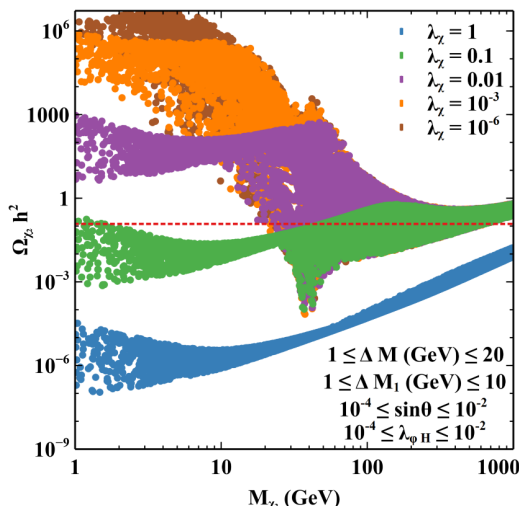
Figure 4. Relic density of DM as a function of DM mass for different values of λ_χ, other parameters being varied randomly as mentioned in the inset.

of a singlet-doublet Dirac fermionic DM include: the mass of the DM (M_{χ_2}), the mass splitting between the dominant singlet and dominant doublet physical states (ΔM), and the mixing angle $(\sin\theta)$. In addition to these three parameters, in the present setup, we have additional parameters that also affect the relic density of DM because of the presence of $\phi_{1,2}$ and ν_R. The presence of $\phi_{1,2}$ in the dark sector leads to additional co-annihilation processes whereas ν_R facilitates a new annihilation channel of DM to RHN. Thus the mass difference between ϕ_2 and χ_2, $(\Delta M_1 = M_{\phi_2} - M_{\chi_2})$, the scalar quartic coupling, $\lambda_{\phi H}$ as well as λ_χ (DM- $\nu_R - \phi_{1,2}$ coupling) also become important parameters in determining the relic density of DM. We have mentioned earlier that the mass difference between physical scalars $(M_{\phi_1} - M_{\phi_2})$ are kept fixed to $1\,\mathrm{GeV}$. So, in this model, we have a multi-dimensional parameter space that decides the relic density of DM. It is worth mentioning here that we used the package MicrOmegas [85] for computing annihilation cross-sections and relic density, after generating the model files using LanHEP [86].

In figure 4, we present the relic density of DM as a function of its mass, considering different benchmark values of λ_χ while randomly varying the other parameters ΔM, ΔM_1, $\sin\theta$, and $\lambda_{\phi H}$ as shown in the inset of the figure. It is evident that an increase in λ_χ results in a gradual decrease in the relic density. This is attributed to the fact that as λ_χ increases, the annihilation cross-section of χ_2 into ν_R also increases. Consequently, the overall effective annihilation cross-section is enhanced, leading to a reduction in the relic density. Additionally, an interesting feature observed in figure 4 is that when λ_χ is not significantly large (i.e., $\lambda_\chi < 0.1$), the relic density of DM is influenced not only by its annihilation into ν_R, but also by other annihilation and co-annihilation processes involving SM particles mediated by the gauge bosons. This explains the resonance features observed around $M_V/2$ $(V \equiv W^\pm, Z)$, represented by the green, purple, orange, and brown points. The Higgs resonance is not prominently visible in this plot because the Higgs-mediated annihilation or co-annihilation channels are less efficient for small $\sin\theta$ and small mass-splitting ΔM. This is attributed to the fact that the corresponding Yukawa coupling y is proportional to $\Delta M \times \sin 2\theta$, as
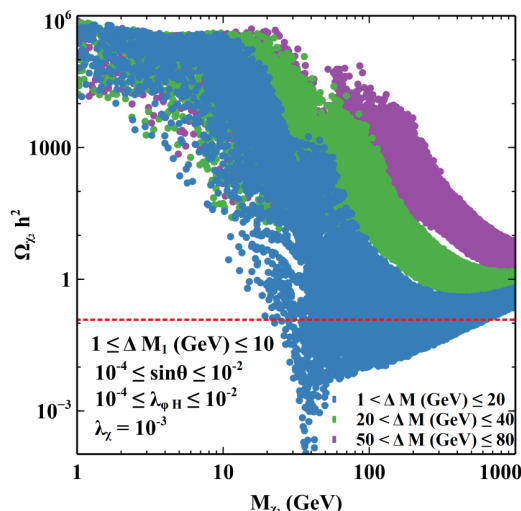
Figure 5. Relic density of DM as a function of DM mass for different values of ΔM, other parameters being varied randomly as mentioned in the inset.

illustrated in eq. (2.6). However, in cases where λ_χ significantly surpasses other couplings, the channel $\chi_2 \chi_2 \to \nu_R \nu_R$ becomes the predominant contributor to the relic density of χ_2. Since this annihilation process occurs through a t-channel, resonance effects are not observed, as indicated by the blue points.

Figure 5 illustrates the correlation between relic density and singlet and doublet mass splitting (ΔM), while mitigating the influence of DM annihilation to ν_Rs by fixing $\lambda_\chi = 10^{-3}$. Other relevant parameters are varied randomly in a specific range as mentioned in the inset. With such a choice of parameters, DM annihilation to ν_R remains subdominant while the DM annihilation to SM particles and co-annihilation of DM with χ_1 and ψ^- dominantly decide the relic abundance. As we can see, with an increase in the mass-splitting ΔM, the relic density decreases and vice versa. This can be understood from eq. (5.2) which is the effective annihilation cross-section of DM. As $\langle \sigma v \rangle_{\text{eff}}$ decreases with an increase in $\Delta_{\chi_1} = \Delta M / M_{\chi_2}$ due to exponential suppression, which consequently elevates the relic density. It is important to note that Δ_{ψ^-} is not an independent parameter but rather is dependent on ΔM and $\sin \theta$.

In figure 6, we depict $\Omega_{\chi_2} h^2$ as a function of M_{χ_2} for various selections of $\lambda_{H\phi}$ to demonstrate the dependency of relic density on this scalar quartic coupling. It is important to note that $\lambda_{H\phi}$ primarily affects the co-annihilation contribution in the effective annihilation cross-section, as it governs the rate of annihilation of $\phi_{1,2}$ as well as co-annihilation of $\phi_{1,2}$ and χ_2 to SM particles. For smaller values of $\lambda_{H\phi}$, we observe that the relic density is not very sensitive. It is only when $\lambda_{\phi H} \sim 1$ that this co-annihilation contribution becomes significant, ultimately influencing the relic density, as indicated by the blue points. The dips in the relic density correspond to resonances corresponding to gauge bosons and the SM Higgs boson.

A common feature observed in all three figures is that in the higher DM mass region, away from resonances, an increase in DM mass leads to a gradual rise in relic density. This phenomenon arises from the fact that in the non-relativistic limit, the effective annihilation cross-section of DM is inversely proportional to its mass. Consequently, as the DM mass increases, $\langle \sigma v \rangle_{\text{eff}}$ decreases, resulting in an increase in relic density.
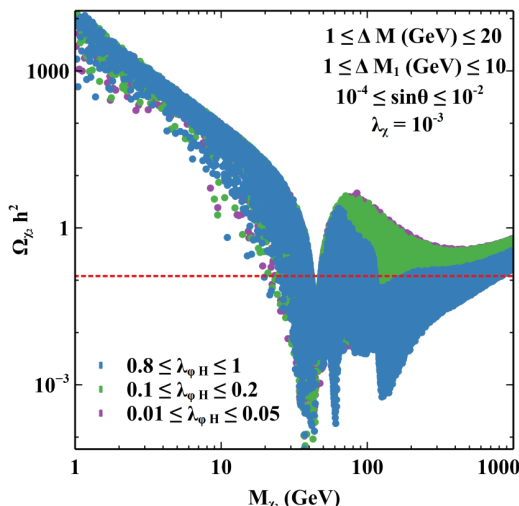
Figure 6. Relic density as a function of DM mass for different ranges of $\lambda_{\phi H}$.

5.2 Direct detection

In this scenario, owing to the singlet-doublet mixing, the DM χ_2 can interact with the target nucleus in terrestrial direct search experiments through Z and Higgs mediated processes. This leads to the cross-section for Z-boson mediated DM-nucleon scattering to be [87, 88]:

$$\sigma^Z_{\text{SI}} = \frac{G_F^2 \sin^4 \theta}{\pi A^2} \mu_r^2 \Big| \left[Z f_p + (A - Z) f_n \right]^2 \Big|^2 \tag{5.5}$$

Where the $f_p = f_n = 0.33$ corresponds to the form factors for proton and neutron, respectively. Here μ_r is the reduced mass of the DM-nucleon system and A, Z are mass number and atomic number respectively. Similarly, the spin-independent DM-nucleon scattering cross-section through Higgs mediation is given by:

$$
\begin{aligned}
\sigma^h_{\text{SI}} = \frac{4}{\pi A^2} \mu_r^2 \frac{y^2 \sin^2 2\theta}{M_h^4} \Big[\frac{m_p}{v} \Big(f^p_{Tu} + f^p_{Td} + f^p_{Ts} + \frac{2}{9} f^p_{TG} \Big) \\
+ \frac{m_n}{v} \Big(f^n_{Tu} + f^n_{Td} + f^n_{Ts} + \frac{2}{9} f^n_{TG} \Big) \Big]^2
\end{aligned}
\tag{5.6}
$$

Different coupling strengths between DM and light quarks are given by [89, 90] $f^p_{Tu} = 0.020 \pm 0.004$, $f^p_{Td} = 0.026 \pm 0.005$, $f^p_{Ts} = 0.014 \pm 0.062$, $f^n_{Tu} = 0.020 \pm 0.004$, $f^n_{Td} = 0.036 \pm 0.005$, $f^n_{Ts} = 0.118 \pm 0.062$. The coupling of DM with the gluons in target nuclei are parameterized by [91] $f^{p,n}_{TG} = 1 - \sum_{q=u,d,s} f^{p,n}_{Tq}$.

Besides these tree-level processes for DM nucleon scattering, there exists another contribution to the spin-independent direct search cross-section, which arises at the loop level with ν_R and $\phi_{1,2}$ in the loop. The corresponding Feynman diagram is as shown in figure 7.

This cross-section can be evaluated as [92]:

$$\sigma^{\text{loop}}_{\text{SI}} = \frac{4}{\pi} \frac{M_{\chi_2}^2 m_p^2}{(M_{\chi_2} + m_p)^2} m_p^2 \, \mathcal{C}^2 \, f_q^2 \tag{5.7}$$
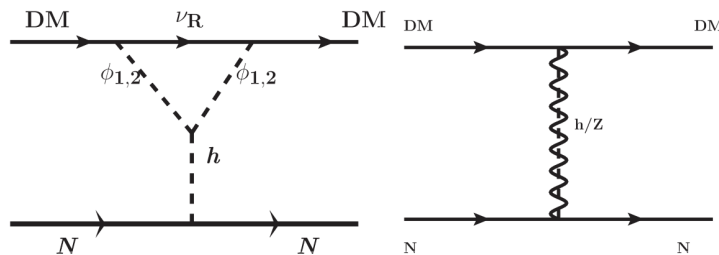
Figure 7. Spin-independent elastic DM-nucleon scattering arising at one loop and tree level.
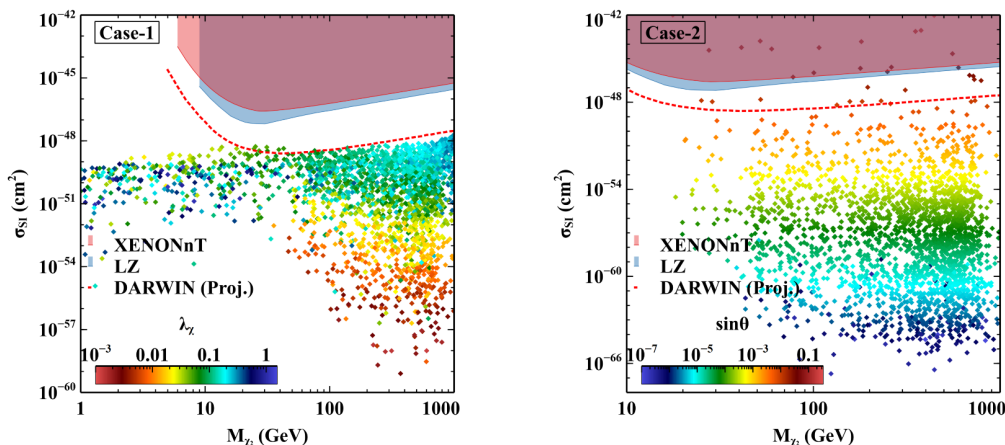

Figure 8. Spin-independent DM-nucleon scattering cross-section as a function of DM mass for case-1(left) and case-2(right).

Where the form factor, $f_q \simeq 0.3$ and the loop-induced effective coupling $\mathcal{C}$ is given by,

$$\mathcal{C} = \frac{\lambda_\chi^2}{16\pi^2 M_h^2 M_{\chi 2}} \lambda_{\phi H} G\left(\frac{M_{\chi 2}^2}{M_\phi^2}\right)$$

And the loop function $G(x)$ is given by,

$$G(x) = \frac{x + (1-x)\ln(1-x)}{x}$$

From eqs. (5.5), (5.6) and (5.7), it is clear that the DM-nucleon interaction strength crucially depends on $\sin\theta$ at tree level, and λ_χ and $\lambda_{\phi H}$ at loop level. Here, it is worth noting that, as λ_χ and $\sin\theta$ are correlated through the neutrino mass constraint as discussed in section 3, depending on their relative strength, the tree level or loop level contribution to DM-nucleon scattering dominates. We scrutinize the model parameters in both cases as mentioned at the beginning of section 5 against the most stringent constraint on DM-nucleon scattering cross-section from XENON-nT [93] and LZ [94] experiments. We also showcase the projected sensitivity of the DARWIN [95]. In case-1 ($\lambda_\chi > 10^{-3}$), because of loop-suppression $\sigma_{\mathrm{SI}}^{\mathrm{loop}}$, as well as because of very small $\sin\theta$, $\sigma_{\mathrm{SI}}^{Z,h}$, remains far below the present sensitivity of LZ and Xenon-nT and hence most of the parameter space remains safe from the DM direct search bounds. This is visible from the left panel of figure 8. In case-2($\lambda_\chi < 10^{-3}$), the one-loop contribution remains suppressed throughout and only the tree-level diagrams

contribute to the DM-nucleon scattering. The right panel of figure 8 clearly illustrates that when $\sin\theta$ is substantial, the interaction strength is correspondingly high, resulting in a large DM-nucleon cross-section. As a result, direct search experiments impose significant constraints on $\sin\theta$. This stringent upper limit is $\sin\theta < 0.03$.

After incorporating the constraints from relic abundance and direct search of DM, now we show the final parameter space in the plane of DM mass and the mass-splittings ΔM and ΔM_1 for the two different cases (Case-1 $[10^{-3} < \lambda_\chi < \sqrt{4\pi}]$ and Case-2$[10^{-11} < \lambda_\chi \le 10^{-3}]$) as mentioned earlier. We also impose the constraints from LEP experiment on the mass of the charged fermion doublet(M_{ψ^-}) i.e. $M_{\psi^-} > 102.7\,\text{GeV}$ and restrict the mass of ϕ_2 to be greater than $M_H/2$ to avoid the constraints from Higgs invisible decay.

Case-1 $[10^{-3} < \lambda_\chi < \sqrt{4\pi}]$. As we know in case-1, characterized by a large value of λ_χ, the primary process determining the correct relic density of χ_2 is $\chi_2\chi_2 \to \nu_R\nu_R$ annihilation. Nevertheless, the contributions from co-annihilation, involving both $\phi_{1,2}$ annihilation to the SM and co-annihilation involving χ_1 and ψ^-, also play crucial roles. These contributions depend on the mass splittings ΔM_1 and ΔM. From the left panel of figure 9, it is evident that as the mass splitting ΔM increases for DM mass $M_{\chi_2} \lesssim 100\,\text{GeV}$, λ_χ must also be raised to attain the correct relic density. This adjustment is necessary because, with an increase in ΔM, the co-annihilation effect gradually diminishes, consequently reducing the effective cross section $\langle\sigma v\rangle_{\text{eff}}$. Therefore, an increase in λ_χ is required to offset this effect and achieve the correct relic density. In the region where $M_{\chi_2} \lesssim 100\,\text{GeV}$ and $\Delta M \lesssim 100\,\text{GeV}$, most of the points shaded in grey are excluded due to the imposed constraint on M_{ψ^-} from the LEP experiment. As we increase the DM mass($M_{\chi_2} \gtrsim 100\,\text{GeV}$), we observe that in the lower mass-splitting region ($\Delta M \lesssim 15\,\text{GeV}$), the mass splitting gradually decreases to achieve the correct relic density. This is because as the DM mass increases, the effective cross section $\langle\sigma v\rangle_{\text{eff}}$ decreases. Consequently, more co-annihilation contribution is required for compensation, necessitating a decrease in ΔM. The region below this always remains under-abundant. In the high DM mass region ($M_{\chi_2} \gtrsim 100\,\text{GeV}$), it becomes evident that λ_χ does not necessarily have to be large. All values of λ_χ are permissible in this region. This is because even if λ_χ is small enough that DM annihilation to ν_R is not highly efficient, the relic density can still be brought to the correct range through various co-annihilation processes.

This understanding gains further support through an analysis of the results as depicted in the right panel of figure 9 by recasting the same points (as shown in the left panel of figure 9), in the plane of ΔM_1 vs M_{χ_2}. By establishing a mass hierarchy among the particles in the dark sector as $M_{\chi_2} < M_{\phi_2} < M_{\phi_1} < M_{\chi_1}$, the co-annihilation processes involving ϕ exert a substantial influence in achieving the correct relic density. Similar to the observations in the left panel of figure 9, as the mass splitting $\Delta M_1(= M_{\phi_2} - M_{\chi_2})$ increases, λ_χ must be augmented to offset the decrease in $\langle\sigma v\rangle_{\text{eff}}$ and thus attain the correct relic density. However, when ΔM_1 is small ($\Delta M_1 < 15\,\text{GeV}$), λ_χ loses its significance, as the relic density is predominantly determined by the co-annihilation processes involving $\phi_{1,2}$. This also clarifies the observed under-abundance in the region below $\Delta M \lesssim 15\,\text{GeV}$ in the left panel of figure 9, since in this scenario, co-annihilation processes involving $\phi_{1,2}$ become overwhelmingly dominant (as $\Delta M_1 < \Delta M$), leading to a significant increase in $\langle\sigma v\rangle_{\text{eff}}$.
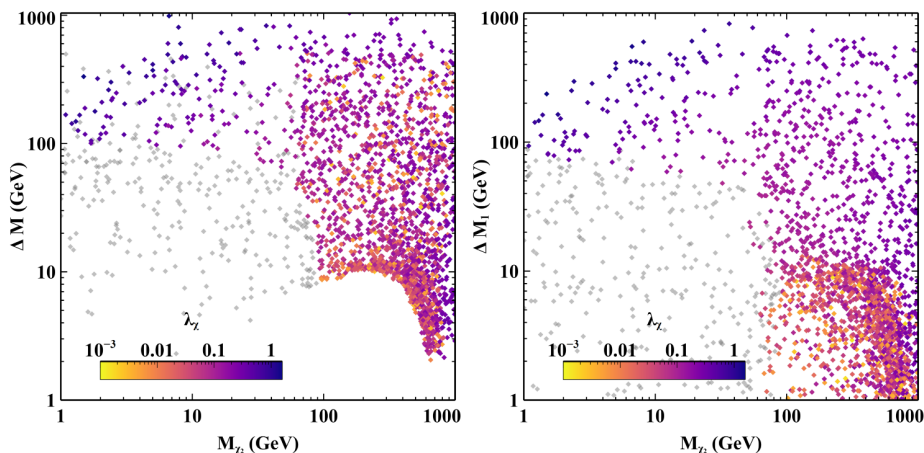
Figure 9. Correct relic density and direct detection constraint satisfying points in the plane of M_{χ_2} and ΔM ([Left]) and in the plane of M_{χ_2} and ΔM_1([Right]). The color code depicts the value of λ_χ. Grey regions are ruled out by the LEP constraint.

Case-2 [$10^{-7} < \lambda_\chi \leq 10^{-3}$]. In this case, λ_χ being very small ($\lambda_\chi < 10^{-3}$), it does not affect the relic density of DM. Rather, DM relic density is completely decided by the co-annihilation of DM with other dark sector particles. As discussed in section 5.2, the stringent limit on $\sin\theta$ is $\sin\theta \lesssim 0.03$ to be consistent with the direct detection constraints. In the most minimal setup of fermionic singlet-doublet DM [52, 72], this crucially crunches the allowed parameter space to $\Delta M < 20\,\text{GeV}$ or so to satisfy correct relic density while being consistent with the direct detection constraints. However, in our setup, we get an enhanced parameter space as compared to this because of the additional channels involving $\phi_{1,2}$ that assist in achieving the correct relic density. Moreover, these points are also not restricted by the direct detection constraints. We show the co-annihilation effects of χ_1, ψ^- and $\phi_{1,2}$ in the plane of ΔM vs M_{χ_2} in the left panel of figure 10. The same points are recast in the plane of ΔM_1 vs M_{χ_2} in the right panel of figure 10. When $\sin\theta$ is small and ΔM is large, the singlet-doublet co-annihilation is not very effective but $\phi_{1,2}$ co-annihilation dominates over the singlet-doublet co-annihilation depending on $\lambda_{\phi H}$ coupling. It is evident from the right panel of figure 10, that when $\lambda_{H\Phi}$ is $\mathcal{O}(1)$, co-annihilations processes involving $\phi_{1,2}$ can significantly contribute to the correct relic density of DM. In either case, the grey coloured points are ruled out due to the LEP constraint.

6 Contribution to ΔN_{eff}

We now focus on the phenomenological consequences that can occur due to the presence of the right-handed counterparts of the SM neutrinos. As mentioned in the earlier section, the Dirac nature of neutrinos necessitates the newly added right-chiral fermions to be as light as the left-handed SM neutrinos. The presence of such additional ultra-light species in the early universe can contribute substantially to the total radiation energy density and hence to the effective relativistic degrees of freedom, N_{eff} which is usually parameterized as

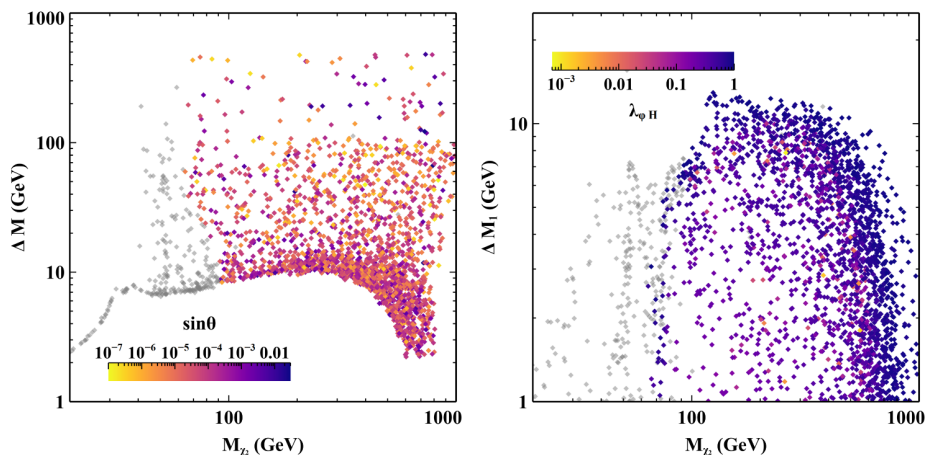$$N_{\text{eff}} \equiv \frac{\rho_{\text{rad}} - \rho_\gamma}{\rho_{\nu_L}}, \tag{6.1}$$

Figure 10. Points satisfying correct relic density and direct detection constraints are shown in the plane of M_{χ_2} and ΔM([Left]) and that in the plane of M_{χ_2} and ΔM_1([Right]). The colour code depicts the value of $\sin\theta$ and $\lambda_{\phi H}$ in the left and right panel figures, respectively.

where $\rho_{\rm rad}$ is the total energy density of the thermal plasma whereas ρ_γ and ρ_{ν_L} are the energy density of photon and single active neutrino species respectively. Without the presence of any new light degrees of freedom, $N_{\rm eff}$ in SM have been calculated very precisely and quoted as 3.045^1 [96–102]. The current data from the observation of cosmic microwave background (CMB) by the Planck satellite [1] suggests $N_{\rm eff} = 2.99^{0.34}_{-0.33}$ at 95% CL (including the baryon acoustic oscillation (BAO) data) which agrees with the SM prediction. The upcoming experiments such as CMB-S4 [82], SPT-3G [103] are expected to be extremely sensitive to $N_{\rm eff}$ and put much more stringent bounds than the Planck experiment due to their potential of exploring all the way down to $\Delta N_{\rm eff} = N_{\rm eff} - N_{\rm eff}^{\rm SM} = 0.06$.

Therefore, $N_{\rm eff}$ is a quantity of immense importance to test the presence of physics beyond SM which can affect CMB and is going to play a crucial role in our discussion. The significance of such contribution may vary depending on whether such light ν_R was present in the thermal bath or produced non-thermally [20, 104, 105]. The connection between the Dirac nature of neutrinos and the origin of DM production has been studied before in [11, 13] in the context of $\Delta N_{\rm eff}$. In this model, ν_R interacts only via Yukawa coupling $\lambda_\chi \overline{\nu_R}\phi\chi$ as shown in the eq. (2.1). Hence, the production of ν_R, whether they were present in the thermal plasma or produced non-thermally with the evolution of our Universe, solely depends on λ_χ. Since we have assumed λ_χ values for the second generation Z_2 odd fermions is much smaller than that of the first generation, the contribution of second generation fermions to $\Delta N_{\rm eff}$ is substantially smaller than the first generation. Therefore, we study the contribution from the first generation Z_2 fermions to $\Delta N_{\rm eff}$ as mentioned by case-1 and case-2 in section 5. From eq. (6.1), the additional contribution to $N_{\rm eff}$ at the time of CMB coming from the presence

---

[1]The deviation from 3 is due to various effects like non-instantaneous neutrino decoupling, flavour oscillations, and finite temperature QED corrections to the electromagnetic plasma [96–102].
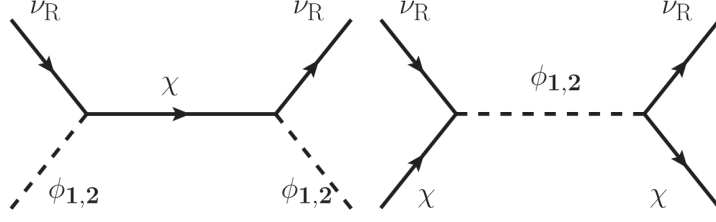
Figure 11. Feynman diagram to keep ν_R in thermal equilibrium.

of ν_R in the total radiation energy density can be written as,

$$\Delta N_{\rm eff} = N_{\nu_R} \times \left. \frac{\rho_{\nu_R}}{\rho_{\nu_L}} \right|_{\rm T=T_{CMB}}, \tag{6.2}$$

where N_{ν_R} is the number of relativistic ν_R species, and ρ_{ν_R} is the energy density of the single ν_R. In the above equation, it is assumed that all three ν_R behave identically, hence contribute equally to the energy density. Depending on the production mechanism of ν_R we will discuss two following cases:

Case-1[$\lambda_\chi > 10^{-3}$]. In this case, the ν_R can be thermally produced in the early universe from the annihilation of χ and ϕ. Figure 11 shows the interactions responsible for keeping ν_R in equilibrium. Once these interaction rates dropped below the expansion rate of the universe, ν_R became decoupled from the thermal plasma and their temperature evolved independently. Hence by using entropy conservation in both sectors, one can write the excess contribution as

$$\Delta N_{\rm eff} = N_{\nu_R} \times \left(\frac{T_{\nu_R}}{T_{\nu_L}} \right)^4 = N_{\nu_R} \left(\frac{g_{*s}(T_{\nu_L}^{\rm dec})}{g_{*s}(T_{\nu_R}^{\rm dec})} \right)^{4/3}, \tag{6.3}$$

where $g_{*s}(T_\kappa^{\rm dec})$ is the relativistic entropy degrees of freedom at temperature $T_\kappa^{\rm dec}$ which is the decoupling temperature of the species $\kappa(=\nu_L, \nu_R)$ from the thermal bath. One important thing to keep in mind is that λ_χ also plays an important role in neutrino mass generation. Increasing λ_χ corresponds to a smaller mixing angle $\sin\theta$ to satisfy the correct neutrino mass. The viable parameter space for $\Delta N_{\rm eff}$ is obtained by satisfying all possible constraints such as neutrino mass, $(g-2)_\mu$ and DM relic density while satisfying direct detection constraints.

Figure 12 shows the variation of $\Delta N_{\rm eff}$ as a function of DM mass ranging from 1 GeV to 1 TeV. The colour gradient shows the dependence on λ_χ. One can clearly see a correlation between $\Delta N_{\rm eff}$, λ_χ and the mass of DM. Larger λ_χ and lighter M_{χ_2} corresponds to larger contribution to the $\Delta N_{\rm eff}$. This can be understood as follows. A larger λ_χ or lighter M_{χ_2} forces χ_2 and hence ν_R to be in thermal bath for longer time. The late decoupling of ν_R from the plasma decreases the denominator in eq. (6.3) and increases its contribution to the $N_{\rm eff}$. The yellow-shaded region is already excluded from the PLANCK 2018 data at 2σ CL. More importantly, future observations of microwave background can test this scenario fully as shown by the pink and orange dashed line, which corresponds to SPT-3G and CMB-S4, respectively. This is because once three of the ν_Rs were produced in the thermal bath of the early Universe, $\Delta N_{\rm eff}$ would always have some minimum contribution of 0.14 which is well above the future prediction from CMB-S4 or SPT-3G. This is the manifestation of the conservation of entropy.
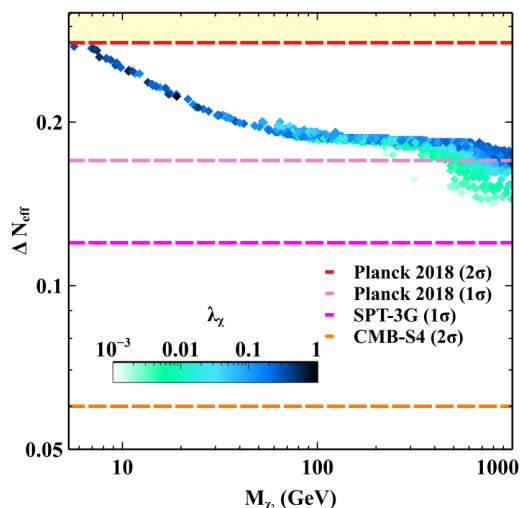
Figure 12. ΔN_{eff} vs DM mass and the colour code is used for λ_χ. The dashed lines show experimental sensitivity, and the shaded region is excluded by Planck 2018 with 2σ sensitivity.
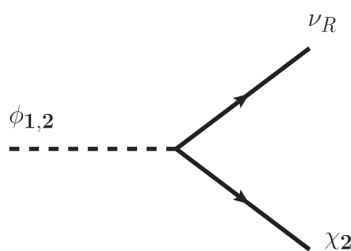

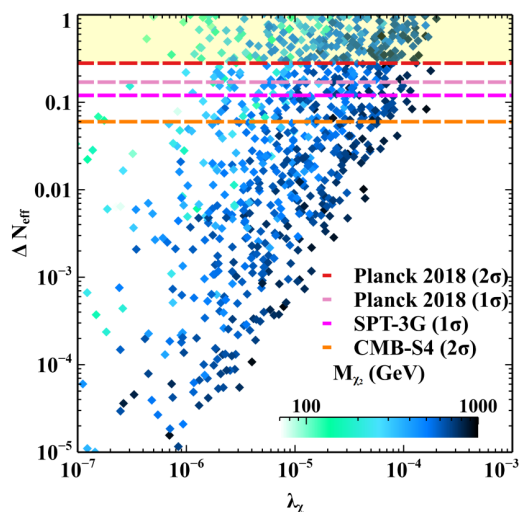**Figure 13.** Production of ν_R from the decay of $\phi_{1,2}$.

Figure 14. ΔN_{eff} vs λ_χ. The colour code is shown for DM mass. Dashed lines show the experimental sensitivity and the shaded region is for the excluded region.

Case-2[$10^{-7} < \lambda_\chi \leq 10^{-3}$]. As discussed above, once the ν_Rs or any light degrees of freedom were thermalized with the SM plasma, there would always be some minimum contribution to the $\Delta N_{\rm eff}$. However, this is not the same in the case of non-thermal production. As we go to the smaller λ_χ, ν_R would no longer be produced in the thermal bath. Rather, they would be produced from the decay of $\phi_{1,2}$ with a χ_2 as shown in figure 13. In this case, we also need to track the evolution of $\phi_{1,2}$ as that will be important to calculate the total energy injected into the radiation energy in terms of light ν_R. We assume that $\phi_{1,2}$ was present in the thermal bath of the early universe and decays both from equilibrium and after freezing out from the thermal bath. So, to track the evolution of ν_R and $\phi_i (i = 1, 2)$ we need to solve the following Boltzmann equations,

$$\frac{dY_{\phi_i}}{dx} = \frac{\beta s}{Hx} \left[-\langle \sigma v \rangle_{\phi_i \phi_i \rightarrow X\bar{X}} (Y_{\phi_i}^2 - (Y_{\phi_i}^{\rm eq})^2) - \frac{\Gamma_{\phi_i}}{s} \frac{K_1(x)}{K_2(x)} Y_{\phi_i} \right]$$

$$\frac{d\tilde{Y}_{\nu_R}}{dx} = \frac{\beta}{Hs^{1/3}x} \langle E\Gamma \rangle Y_{\phi_i}, \tag{6.4}$$

where the dimensionless parameters $Y_{\phi_i} = \sum_{i=1}^2 n_{\phi_i}/s$ and $\tilde{Y}_{\nu_R} = \rho_{\nu_R}/s^{4/3}$. In the above equation Γ_{ϕ_i} and $\langle E\Gamma \rangle$ can be expressed as

$$\Gamma(\phi_i \rightarrow \chi\nu_R) = \frac{1}{8\pi} \lambda_\chi^2 \cos\theta^2 M_{\phi_i} \left(1 - \frac{M_{\chi_2}^2}{M_{\phi_i^2}} \right)^2 \tag{6.5}$$

$$\langle E\Gamma(\phi_i \rightarrow \chi\nu_R) \rangle = \frac{1}{16\pi} \lambda_\chi^2 \cos\theta^2 M_{\phi_i}^2 \left(1 - \frac{M_{\chi_2}^2}{M_{\phi_i^2}} \right)^3. \tag{6.6}$$

After solving the above Boltzmann equations, $\Delta N_{\rm eff}$ produced by ρ_{ν_R} can be calculated as:

$$\Delta N_{\rm eff} = 3 \times 2 \left(\frac{\rho_{\nu_R}}{\rho_{\nu_L}} \right)_{T_D(\nu_L)}$$

$$= 6 \left(\frac{s^{4/3} \tilde{Y}_{\nu_R}}{\rho_{\nu_L}} \right)_{T_D(\nu_L)} \tag{6.7}$$

The factor of 3 in eq. (6.7) corresponds to the three generations of ν_R and 2 incorporates both particles and antiparticles. Figure 14 shows the variation of $\Delta N_{\rm eff}$ as a function of λ_χ where the colour bar represents the variation of M_{χ_2}. We have considered the mass difference between ϕ_2 and χ_2 to be $\leq 10 \, {\rm GeV}$. Eq. (6.6) says that with larger λ_χ, the decay width of $\phi_{1,2}$ will increase and hence more RHNs will be produced. If we increase the DM mass, the factor inside the bracket will decrease, hence the decay width will decrease. We can see $\Delta N_{\rm eff}$ increases with λ_χ and for a fixed λ_χ, it decreases with increase in M_{χ_2}. One can note that some part of the parameter space is excluded from the present PLANCK data and future experiments can probe some part of it. However, for smaller λ_χ, $\Delta N_{\rm eff}$ becomes extremely small and drops well below the future projections of CMB-S4 or SPT-3G limits.

7 Conclusion

In this study, we delved into a singlet-doublet fermionic DM model that offers a scotogenic avenue for generating Dirac neutrino masses. To achieve this, we extended the basic singlet-doublet DM framework by introducing an additional singlet scalar and the right-chiral

components of neutrinos, ν_Rs. This extension also aids in addressing the $(g-2)_\mu$ anomaly, with a positive contribution arising from the one-loop diagram mediated by the charged fermion doublet ψ^- and $\phi_{1,2}$. Following the inclusion of constraints stemming from neutrino mass, $(g-2)_\mu$, and lepton flavour violation (LFV), we conducted a comprehensive exploration of the DM phenomenology.

In the analysis of DM, we delineated two distinct cases for examination, based on the thermalisation criteria of ν_R, as this can yield intriguing implications from the perspective of the additional effective neutrino species ($\Delta N_{\rm eff}$). We find an enhanced parameter space because of the presence of $\phi_{1,2}$ in the dark sector as it helps in achieving correct relic density due to additional co-annihilation contributions. We considered both tree-level and loop-level DM-nucleon scattering possibilities for the DM direct detection perspectives. While direct DM search experiments do not impose stringent restrictions on the model parameters, $\Delta N_{\rm eff}$ offers an additional cosmological probe for the model. As ν_R is connected to the thermal bath, only through the dark sector particles, in the scenario, where ν_R is thermalized, future CMB experiment SPT-3G can probe the higher DM mass range of the model whereas when ν_R is produced non-thermally, both SPT-3G and CMB-S4 can probe significant portion of the model parameter space.

Acknowledgments

A Lagrangian

Following from eq. (2.1), we can write the Lagrangian in terms of physical states as,

$$
\begin{aligned}
\mathcal{L}_{\rm int}^{\rm DM} &= i\overline{\psi}\gamma^\mu\left(\partial_\mu - g\frac{\tau_i}{2}W^i_\mu - g'\frac{Y}{2}B_\mu\right)\Psi + i\overline{\chi}\gamma^\mu\partial_\mu\chi - (\lambda_\psi \overline{L}\phi\Psi + \lambda_\chi \overline{\nu_R}\phi\chi + {\rm h.c.})\\
\mathcal{L}_{\rm int}^{\rm DM} &= g_Z\Big[\sin^2\theta\overline{\chi_2}\gamma^\mu Z_\mu\chi_2 + \cos^2\theta\overline{\chi_1}\gamma^\mu Z_\mu\chi_1 + \sin\theta\cos\theta(\overline{\chi_1}\gamma^\mu Z_\mu\chi_2 + \overline{\chi_2}\gamma^\mu Z_\mu\chi_1)\Big]\\
&\quad + g_W(\sin\theta\overline{\chi_2}\gamma^\mu W^+_\mu\psi^- + \cos\theta\overline{\chi_1}\gamma^\mu W^+_\mu\psi^-) + g_W(\sin\theta\psi^+\gamma^\mu W^-_\mu\chi_2 + \cos\theta\psi^+\gamma^\mu W^-_\mu\chi_1)\\
&\quad - g_Z\,c_{2w}\,\psi^+\gamma^\mu Z_\mu\psi^- - e_0\psi^+\gamma^\mu A_\mu\psi^- - \lambda_\psi \overline{e_L}\phi\psi^-\\
&\quad - \Big[\cos\theta(\lambda_\psi \overline{\nu_L}\phi\chi_1 + \lambda_\chi \overline{\nu_R}\phi\chi_2) + \sin\theta(\lambda_\chi \overline{\nu_R}\phi\chi_1 - \lambda_\psi \overline{\nu_L}\phi\chi_2)\Big]
\end{aligned}
\tag{A.1}
$$

where $g_Z = e_0/2s_w c_w$, $g_W = e_0/\sqrt{2}s_w$ and s_w, c_w, c_{2w} denote $\sin\theta_W$ and $\cos\theta_W$ and $\cos 2\theta_W$ respectively.

References

[1] PLANCK collaboration, *Planck* 2018 *results. VI. Cosmological parameters*, *Astron. Astrophys.* **641** (2020) A6 [*Erratum ibid.* **652** (2021) C4] [`arXiv:1807.06209`] [INSPIRE].

[2] WMAP collaboration, *Nine-year Wilkinson Microwave Anisotropy Probe (WMAP) observations: cosmological parameter results*, *Astrophys. J. Suppl.* **208** (2013) 19 [`arXiv:1212.5226`] [INSPIRE].

[3] B.W. Lee and S. Weinberg, *Cosmological lower bound on heavy neutrino masses*, *Phys. Rev. Lett.* **39** (1977) 165 [INSPIRE].

[4] K. Griest and M. Kamionkowski, *Unitarity limits on the mass and radius of dark matter particles*, *Phys. Rev. Lett.* **64** (1990) 615 [INSPIRE].

[5] SUPER-KAMIOKANDE collaboration, *Evidence for oscillation of atmospheric neutrinos*, *Phys. Rev. Lett.* **81** (1998) 1562 [`hep-ex/9807003`] [INSPIRE].

[6] SNO collaboration, *Measurement of the rate of $\nu_e + d \rightarrow p + p + e^-$ interactions produced by ^8B solar neutrinos at the Sudbury Neutrino Observatory*, *Phys. Rev. Lett.* **87** (2001) 071301 [`nucl-ex/0106015`] [INSPIRE].

[7] DOUBLE CHOOZ collaboration, *Indication of reactor $\bar{\nu}_e$ disappearance in the double Chooz experiment*, *Phys. Rev. Lett.* **108** (2012) 131801 [`arXiv:1112.6353`] [INSPIRE].

[8] DAYA BAY collaboration, *Observation of electron-antineutrino disappearance at Daya Bay*, *Phys. Rev. Lett.* **108** (2012) 171803 [`arXiv:1203.1669`] [INSPIRE].

[9] RENO collaboration, *Observation of Reactor Electron Antineutrino Disappearance in the RENO experiment*, *Phys. Rev. Lett.* **108** (2012) 191802 [`arXiv:1204.0626`] [INSPIRE].

[10] PARTICLE DATA GROUP collaboration, *Review of particle physics*, *PTEP* **2022** (2022) 083C01 [INSPIRE].

[11] A. Biswas, D. Borah and D. Nanda, *Light Dirac neutrino portal dark matter with observable ΔN_{eff}*, *JCAP* **10** (2021) 002 [`arXiv:2103.05648`] [INSPIRE].

[12] D. Borah, S. Mahapatra, D. Nanda and N. Sahu, *Type II Dirac seesaw with observable ΔN_{eff} in the light of W-mass anomaly*, *Phys. Lett. B* **833** (2022) 137297 [`arXiv:2204.08266`] [INSPIRE].

[13] A. Biswas, D. Borah, N. Das and D. Nanda, *Freeze-in dark matter via a light Dirac neutrino portal*, *Phys. Rev. D* **107** (2023) 015015 [`arXiv:2205.01144`] [INSPIRE].

[14] E. Ma and O. Popov, *Pathways to naturally small Dirac neutrino masses*, *Phys. Lett. B* **764** (2017) 142 [`arXiv:1609.02538`] [INSPIRE].

[15] C.-Y. Yao and G.-J. Ding, *Systematic study of one-loop Dirac neutrino masses and viable dark matter candidates*, *Phys. Rev. D* **96** (2017) 095004 [*Erratum ibid.* **98** (2018) 039901] [`arXiv:1707.09786`] [INSPIRE].

[16] C.D.R. Carvajal and Ó. Zapata, *One-loop Dirac neutrino mass and mixed axion-WIMP dark matter*, *Phys. Rev. D* **99** (2019) 075009 [`arXiv:1812.06364`] [INSPIRE].

[17] S. Jana, P.K. Vishnu and S. Saad, *Minimal realizations of Dirac neutrino mass from generic one-loop and two-loop topologies at $d = 5$*, *JCAP* **04** (2020) 018 [`arXiv:1910.09537`] [INSPIRE].

[18] D. Nanda and D. Borah, *Connecting light Dirac neutrinos to a multi-component dark matter scenario in gauged B − L model*, *Eur. Phys. J. C* **80** (2020) 557 [arXiv:1911.04703] [InSPIRE].

[19] D. Borah, S. Mahapatra, D. Nanda and N. Sahu, *Inelastic fermion dark matter origin of XENON1T excess with muon (g − 2) and light neutrino mass*, *Phys. Lett. B* **811** (2020) 135933 [arXiv:2007.10754] [InSPIRE].

[20] A. Biswas, D.K. Ghosh and D. Nanda, *Concealing Dirac neutrinos from cosmic microwave background*, *JCAP* **10** (2022) 006 [arXiv:2206.13710] [InSPIRE].

[21] W. Wang and Z.-L. Han, *Naturally small Dirac neutrino mass with intermediate* $\mathrm{SU}(2)_L$ *multiplet fields*, *JHEP* **04** (2017) 166 [arXiv:1611.03240] [InSPIRE].

[22] T. Aoyama, M. Hayakawa, T. Kinoshita and M. Nio, *Complete tenth-order QED contribution to the muon g − 2*, *Phys. Rev. Lett.* **109** (2012) 111808 [arXiv:1205.5370] [InSPIRE].

[23] T. Aoyama, T. Kinoshita and M. Nio, *Theory of the anomalous magnetic moment of the electron*, *Atoms* **7** (2019) 28 [InSPIRE].

[24] A. Czarnecki, W.J. Marciano and A. Vainshtein, *Refinements in electroweak contributions to the muon anomalous magnetic moment*, *Phys. Rev. D* **67** (2003) 073006 [*Erratum ibid.* **73** (2006) 119901] [hep-ph/0212229] [InSPIRE].

[25] C. Gnendiger, D. Stöckinger and H. Stöckinger-Kim, *The electroweak contributions to* $(g − 2)_\mu$ *after the Higgs boson mass measurement*, *Phys. Rev. D* **88** (2013) 053005 [arXiv:1306.5546] [InSPIRE].

[26] M. Davier, A. Hoecker, B. Malaescu and Z. Zhang, *Reevaluation of the hadronic vacuum polarisation contributions to the Standard Model predictions of the muon g − 2 and* $\alpha(m_Z^2)$ *using newest hadronic cross-section data*, *Eur. Phys. J. C* **77** (2017) 827 [arXiv:1706.09436] [InSPIRE].

[27] A. Keshavarzi, D. Nomura and T. Teubner, *Muon g − 2 and* $\alpha(M_Z^2)$: *a new data-based analysis*, *Phys. Rev. D* **97** (2018) 114025 [arXiv:1802.02995] [InSPIRE].

[28] G. Colangelo, M. Hoferichter and P. Stoffer, *Two-pion contribution to hadronic vacuum polarization*, *JHEP* **02** (2019) 006 [arXiv:1810.00007] [InSPIRE].

[29] M. Hoferichter, B.-L. Hoid and B. Kubis, *Three-pion contribution to hadronic vacuum polarization*, *JHEP* **08** (2019) 137 [arXiv:1907.01556] [InSPIRE].

[30] M. Davier, A. Hoecker, B. Malaescu and Z. Zhang, *A new evaluation of the hadronic vacuum polarisation contributions to the muon anomalous magnetic moment and to* $\alpha(m_Z^2)$, *Eur. Phys. J. C* **80** (2020) 241 [*Erratum ibid.* **80** (2020) 410] [arXiv:1908.00921] [InSPIRE].

[31] A. Keshavarzi, D. Nomura and T. Teubner, *g − 2 of charged leptons,* $\alpha(M_Z^2)$, *and the hyperfine splitting of muonium*, *Phys. Rev. D* **101** (2020) 014029 [arXiv:1911.00367] [InSPIRE].

[32] A. Kurz, T. Liu, P. Marquard and M. Steinhauser, *Hadronic contribution to the muon anomalous magnetic moment to next-to-next-to-leading order*, *Phys. Lett. B* **734** (2014) 144 [arXiv:1403.6400] [InSPIRE].

[33] K. Melnikov and A. Vainshtein, *Hadronic light-by-light scattering contribution to the muon anomalous magnetic moment revisited*, *Phys. Rev. D* **70** (2004) 113006 [hep-ph/0312226] [InSPIRE].

[34] P. Masjuan and P. Sanchez-Puertas, *Pseudoscalar-pole contribution to the* $(g_\mu − 2)$: *a rational approach*, *Phys. Rev. D* **95** (2017) 054026 [arXiv:1701.05829] [InSPIRE].

[35] G. Colangelo, M. Hoferichter, M. Procura and P. Stoffer, *Dispersion relation for hadronic light-by-light scattering: two-pion contributions*, *JHEP* **04** (2017) 161 [arXiv:1702.07347] [INSPIRE].

[36] M. Hoferichter et al., *Dispersion relation for hadronic light-by-light scattering: pion pole*, *JHEP* **10** (2018) 141 [arXiv:1808.04823] [INSPIRE].

[37] A. Gérardin, H.B. Meyer and A. Nyffeler, *Lattice calculation of the pion transition form factor with $N_f = 2 + 1$ Wilson quarks*, *Phys. Rev. D* **100** (2019) 034520 [arXiv:1903.09471] [INSPIRE].

[38] J. Bijnens, N. Hermansson-Truedsson and A. Rodríguez-Sánchez, *Short-distance constraints for the HLbL contribution to the muon anomalous magnetic moment*, *Phys. Lett. B* **798** (2019) 134994 [arXiv:1908.03331] [INSPIRE].

[39] G. Colangelo et al., *Longitudinal short-distance constraints for the hadronic light-by-light contribution to $(g-2)_\mu$ with large-N_c Regge models*, *JHEP* **03** (2020) 101 [arXiv:1910.13432] [INSPIRE].

[40] T. Blum et al., *Hadronic light-by-light scattering contribution to the muon anomalous magnetic moment from lattice QCD*, *Phys. Rev. Lett.* **124** (2020) 132002 [arXiv:1911.08123] [INSPIRE].

[41] G. Colangelo et al., *Remarks on higher-order hadronic corrections to the muon $g-2$*, *Phys. Lett. B* **735** (2014) 90 [arXiv:1403.7512] [INSPIRE].

[42] A.L. Cherchiglia, G. De Conto and C.C. Nishi, *Connecting $(g-2)_\mu$ to neutrino mass in the extended neutrinophilic 2HDM*, *JHEP* **08** (2023) 170 [arXiv:2304.00038] [INSPIRE].

[43] A. Crivellin and M. Hoferichter, *Consequences of chirally enhanced explanations of $(g-2)_\mu$ for $h \to \mu\mu$ and $Z \to \mu\mu$*, *JHEP* **07** (2021) 135 [*Erratum ibid.* **10** (2022) 030] [arXiv:2104.03202] [INSPIRE].

[44] A. Crivellin, M. Hoferichter and P. Schmidt-Wellenburg, *Combined explanations of $(g-2)_{\mu,e}$ and implications for a large muon EDM*, *Phys. Rev. D* **98** (2018) 113002 [arXiv:1807.11484] [INSPIRE].

[45] MUON G-2 collaboration, *Measurement of the positive muon anomalous magnetic moment to 0.20 ppm*, *Phys. Rev. Lett.* **131** (2023) 161802 [arXiv:2308.06230] [INSPIRE].

[46] T. Aoyama et al., *The anomalous magnetic moment of the muon in the Standard Model*, *Phys. Rept.* **887** (2020) 1 [arXiv:2006.04822] [INSPIRE].

[47] CMD-3 collaboration, *Measurement of the $e^+e^- \to \pi^+\pi^-$ cross section from threshold to 1.2 GeV with the CMD-3 detector*, arXiv:2302.08834 [INSPIRE].

[48] F. Jegerlehner and A. Nyffeler, *The muon $g-2$*, *Phys. Rept.* **477** (2009) 1 [arXiv:0902.3360] [INSPIRE].

[49] M. Lindner, M. Platscher and F.S. Queiroz, *A call for new physics: the muon anomalous magnetic moment and lepton flavor violation*, *Phys. Rept.* **731** (2018) 1 [arXiv:1610.06587] [INSPIRE].

[50] P. Athron et al., *New physics explanations of a_μ in light of the FNAL muon $g-2$ measurement*, *JHEP* **09** (2021) 080 [arXiv:2104.03691] [INSPIRE].

[51] S. Bhattacharya, N. Sahoo and N. Sahu, *Minimal vectorlike leptonic dark matter and signatures at the LHC*, *Phys. Rev. D* **93** (2016) 115040 [arXiv:1510.02760] [INSPIRE].

[52] S. Bhattacharya, P. Ghosh, N. Sahoo and N. Sahu, *Mini review on vector-like leptonic dark matter, neutrino mass, and collider signatures*, *Front. in Phys.* **7** (2019) 80 [arXiv:1812.06505] [INSPIRE].

[53] S. Banerjee, S. Matsumoto, K. Mukaida and Y.-L.S. Tsai, *WIMP dark matter in a well-tempered regime: a case study on singlet-doublets fermionic WIMP*, *JHEP* **11** (2016) 070 [arXiv:1603.07387] [INSPIRE].

[54] A. Dutta Banik, A.K. Saha and A. Sil, *Scalar assisted singlet doublet fermion dark matter model and electroweak vacuum stability*, *Phys. Rev. D* **98** (2018) 075013 [arXiv:1806.08080] [INSPIRE].

[55] S. Horiuchi et al., *The Fermi-LAT gamma-ray excess at the galactic center in the singlet-doublet fermion dark matter model*, *JCAP* **03** (2016) 048 [arXiv:1602.04788] [INSPIRE].

[56] D. Restrepo et al., *Radiative neutrino masses in the singlet-doublet fermion dark matter model with scalar singlets*, *Phys. Rev. D* **92** (2015) 013005 [arXiv:1504.07892] [INSPIRE].

[57] M. Badziak, M. Olechowski and P. Szczerbiak, *Is well-tempered neutralino in MSSM still alive after* 2016 *LUX results?*, *Phys. Lett. B* **770** (2017) 226 [arXiv:1701.05869] [INSPIRE].

[58] A. Betancur, G. Palacio and A. Rivera, *Inert doublet as multicomponent dark matter*, *Nucl. Phys. B* **962** (2021) 115276 [arXiv:2002.02036] [INSPIRE].

[59] T. Abe, *Effect of CP violation in the singlet-doublet dark matter model*, *Phys. Lett. B* **771** (2017) 125 [arXiv:1702.07236] [INSPIRE].

[60] T. Abe and R. Sato, *Current status and future prospects of the singlet-doublet dark matter model with CP-violation*, *Phys. Rev. D* **99** (2019) 035012 [arXiv:1901.02278] [INSPIRE].

[61] B. Barman et al., *Fermion dark matter with scalar triplet at direct and collider searches*, *Phys. Rev. D* **100** (2019) 015027 [arXiv:1902.01217] [INSPIRE].

[62] L. Calibbi, L. Lopez-Honorez, S. Lowette and A. Mariotti, *Singlet-doublet dark matter freeze-in: LHC displaced signatures versus cosmology*, *JHEP* **09** (2018) 037 [arXiv:1805.04423] [INSPIRE].

[63] K. Fraser, A. Parikh and W.L. Xu, *A closer look at CP-violating Higgs portal dark matter as a candidate for the GCE*, *JHEP* **03** (2021) 123 [arXiv:2010.15129] [INSPIRE].

[64] A. Freitas, S. Westhoff and J. Zupan, *Integrating in the Higgs portal to fermion dark matter*, *JHEP* **09** (2015) 015 [arXiv:1506.04149] [INSPIRE].

[65] G. Cynolter, J. Kovács and E. Lendvai, *Doublet-singlet model and unitarity*, *Mod. Phys. Lett. A* **31** (2016) 1650013 [arXiv:1509.05323] [INSPIRE].

[66] L. Calibbi, A. Mariotti and P. Tziveloglou, *Singlet-doublet model: dark matter searches and LHC constraints*, *JHEP* **10** (2015) 116 [arXiv:1505.03867] [INSPIRE].

[67] T. Abe, R. Kitano and R. Sato, *Discrimination of dark matter models in future experiments*, *Phys. Rev. D* **91** (2015) 095004 [*Erratum ibid.* **96** (2017) 019902] [arXiv:1411.1335] [INSPIRE].

[68] C. Cheung and D. Sanford, *Simplified models of mixed dark matter*, *JCAP* **02** (2014) 011 [arXiv:1311.5896] [INSPIRE].

[69] T. Cohen, J. Kearney, A. Pierce and D. Tucker-Smith, *Singlet-doublet dark matter*, *Phys. Rev. D* **85** (2012) 075003 [arXiv:1109.2604] [INSPIRE].

[70] M. Dutta, S. Bhattacharya, P. Ghosh and N. Sahu, *Majorana dark matter and neutrino mass in a singlet-doublet extension of the standard model*, *Springer Proc. Phys.* **277** (2022) 685 [arXiv:2106.13857] [INSPIRE].

[71] P. Ghosh and S. Jeesun, *Reviving sub-TeV* SU(2)$_L$ *lepton doublet dark matter*, *Eur. Phys. J. C* **83** (2023) 880 [arXiv:2306.12906] [INSPIRE].

[72] D. Borah, M. Dutta, S. Mahapatra and N. Sahu, *Lepton anomalous magnetic moment with singlet-doublet fermion dark matter in a scotogenic* U(1)$_{L_\mu - L_\tau}$ *model*, *Phys. Rev. D* **105** (2022) 015029 [arXiv:2109.02699] [INSPIRE].

[73] S. Bhattacharya, S. Jahedi and J. Wudka, *Probing heavy charged fermions at* e^+e^- *collider using the optimal observable technique*, *JHEP* **05** (2022) 009 [arXiv:2106.02846] [INSPIRE].

[74] S. Bhattacharya, P. Ghosh and N. Sahu, *Multipartite dark matter with scalars, fermions and signatures at LHC*, *JHEP* **02** (2019) 059 [arXiv:1809.07474] [INSPIRE].

[75] S. Bhattacharya, B. Karmakar, N. Sahu and A. Sil, *Flavor origin of dark matter and its relation with leptonic nonzero* θ_{13} *and Dirac CP phase* δ, *JHEP* **05** (2017) 068 [arXiv:1611.07419] [INSPIRE].

[76] S. Bhattacharya, N. Sahoo and N. Sahu, *Singlet-doublet fermionic dark matter, neutrino mass and collider signatures*, *Phys. Rev. D* **96** (2017) 035010 [arXiv:1704.03417] [INSPIRE].

[77] M. Dutta, S. Bhattacharya, P. Ghosh and N. Sahu, *Singlet-doublet Majorana dark matter and neutrino mass in a minimal type-I seesaw scenario*, *JCAP* **03** (2021) 008 [arXiv:2009.00885] [INSPIRE].

[78] P. Konar, A. Mukherjee, A.K. Saha and S. Show, *Linking pseudo-Dirac dark matter to radiative neutrino masses in a singlet-doublet scenario*, *Phys. Rev. D* **102** (2020) 015024 [arXiv:2001.11325] [INSPIRE].

[79] P. Konar, A. Mukherjee, A.K. Saha and S. Show, *A dark clue to seesaw and leptogenesis in a pseudo-Dirac singlet doublet scenario with (non)standard cosmology*, *JHEP* **03** (2021) 044 [arXiv:2007.15608] [INSPIRE].

[80] D. Borah, S. Mahapatra and N. Sahu, *Singlet-doublet fermion origin of dark matter, neutrino mass and W-mass anomaly*, *Phys. Lett. B* **831** (2022) 137196 [arXiv:2204.09671] [INSPIRE].

[81] D. Borah, M. Dutta, S. Mahapatra and N. Sahu, *Singlet-doublet self-interacting dark matter and radiative neutrino mass*, *Phys. Rev. D* **105** (2022) 075019 [arXiv:2112.06847] [INSPIRE].

[82] K. Abazajian et al., *CMB-S4 science case, reference design, and project plan*, arXiv:1907.04473 [INSPIRE].

[83] R. Barbieri, A. Pomarol, R. Rattazzi and A. Strumia, *Electroweak symmetry breaking after LEP-1 and LEP-2*, *Nucl. Phys. B* **703** (2004) 127 [hep-ph/0405040] [INSPIRE].

[84] MEG collaboration, *Search for the lepton flavour violating decay* $\mu^+ \to e^+\gamma$ *with the full dataset of the MEG experiment*, *Eur. Phys. J. C* **76** (2016) 434 [arXiv:1605.05081] [INSPIRE].

[85] G. Bélanger, F. Boudjema, A. Pukhov and A. Semenov, *microOMEGAs4.1: two dark matter candidates*, *Comput. Phys. Commun.* **192** (2015) 322 [arXiv:1407.6129] [INSPIRE].

[86] A. Semenov, *LanHEP: a package for the automatic generation of Feynman rules in field theory. Version 3.0*, *Comput. Phys. Commun.* **180** (2009) 431 [arXiv:0805.0555] [INSPIRE].

[87] M.W. Goodman and E. Witten, *Detectability of certain dark matter candidates*, *Phys. Rev. D* **31** (1985) 3059 [INSPIRE].

[88] R. Essig, *Direct detection of non-chiral dark matter*, *Phys. Rev. D* **78** (2008) 015004 [arXiv:0710.1668] [INSPIRE].

[89] G. Bertone, D. Hooper and J. Silk, *Particle dark matter: evidence, candidates and constraints*, *Phys. Rept.* **405** (2005) 279 [hep-ph/0404175] [INSPIRE].

[90] J.M. Alarcon, L.S. Geng, J. Martin Camalich and J.A. Oller, *The strangeness content of the nucleon from effective field theory and phenomenology*, *Phys. Lett. B* **730** (2014) 342 [arXiv:1209.2870] [InSPIRE].

[91] M. Hoferichter, P. Klos, J. Menéndez and A. Schwenk, *Improved limits for Higgs-portal dark matter from LHC searches*, *Phys. Rev. Lett.* **119** (2017) 181803 [arXiv:1708.02245] [InSPIRE].

[92] A. Ibarra, C.E. Yaguna and O. Zapata, *Direct detection of fermion dark matter in the radiative seesaw model*, *Phys. Rev. D* **93** (2016) 035012 [arXiv:1601.01163] [InSPIRE].

[93] XENON collaboration, *First dark matter search with nuclear recoils from the XENONnT experiment*, *Phys. Rev. Lett.* **131** (2023) 041003 [arXiv:2303.14729] [InSPIRE].

[94] LZ collaboration, *First dark matter search results from the LUX-ZEPLIN (LZ) experiment*, *Phys. Rev. Lett.* **131** (2023) 041002 [arXiv:2207.03764] [InSPIRE].

[95] DARWIN collaboration, *DARWIN: towards the ultimate dark matter detector*, *JCAP* **11** (2016) 017 [arXiv:1606.07001] [InSPIRE].

[96] G. Mangano et al., *Relic neutrino decoupling including flavor oscillations*, *Nucl. Phys. B* **729** (2005) 221 [hep-ph/0506164] [InSPIRE].

[97] E. Grohs et al., *Neutrino energy transport in weak decoupling and big bang nucleosynthesis*, *Phys. Rev. D* **93** (2016) 083522 [arXiv:1512.02205] [InSPIRE].

[98] P.F. de Salas and S. Pastor, *Relic neutrino decoupling with flavour oscillations revisited*, *JCAP* **07** (2016) 051 [arXiv:1606.06986] [InSPIRE].

[99] M. Cielo, M. Escudero, G. Mangano and O. Pisanti, $N_{\rm eff}$ *in the standard model at NLO is* 3.043, *Phys. Rev. D* **108** (2023) L121301 [arXiv:2306.05460] [InSPIRE].

[100] K. Akita and M. Yamaguchi, *A precision calculation of relic neutrino decoupling*, *JCAP* **08** (2020) 012 [arXiv:2005.07047] [InSPIRE].

[101] J. Froustey, C. Pitrou and M.C. Volpe, *Neutrino decoupling including flavour oscillations and primordial nucleosynthesis*, *JCAP* **12** (2020) 015 [arXiv:2008.01074] [InSPIRE].

[102] J.J. Bennett et al., *Towards a precision calculation of $N_{\rm eff}$ in the Standard Model II: neutrino decoupling in the presence of flavour oscillations and finite-temperature QED*, *JCAP* **04** (2021) 073 [arXiv:2012.02726] [InSPIRE].

[103] SPT-3G collaboration, *Particle physics with the cosmic microwave background with SPT-3G*, *J. Phys. Conf. Ser.* **1468** (2020) 012008 [arXiv:1911.08047] [InSPIRE].

[104] X. Luo, W. Rodejohann and X.-J. Xu, *Dirac neutrinos and $N_{\rm eff}$*, *JCAP* **06** (2020) 058 [arXiv:2005.01629] [InSPIRE].

[105] X. Luo, W. Rodejohann and X.-J. Xu, *Dirac neutrinos and $N_{\rm eff}$. Part II. The freeze-in case*, *JCAP* **03** (2021) 082 [arXiv:2011.13059] [InSPIRE].